


Repetitive Mild Closed Head Injury in Adolescent Mice Is Associated with Impaired Proteostasis, Neuroinflammation, and Tauopathy

Limin Wu,¹ Brian T. Kalish,^{2,3,4,5} Benjamin Finander,^{2,3} Tian Cao,^{1,6} Gina Jin,¹ Taha Yahya,¹  Emily S. Levy,¹ Bharti Kukreja,⁴ Eliza Sophie LaRovere,¹ Joon Yong Chung,¹ Eng H. Lo,^{7,8} Alexander Brown-Whalen,⁹ Joseph El Khoury,⁹ David L. Kaplan,¹⁰ and Michael J. Whalen¹

¹Department of Pediatrics, Massachusetts General Hospital, Harvard Medical School, Boston, Massachusetts 02114, ²Department of Neurobiology, Harvard Medical School, Boston, Massachusetts 02115, ³Division of Newborn Medicine, Department of Medicine, Boston Children's Hospital, Boston, Massachusetts 02115, ⁴Program in Neuroscience and Mental Health, SickKids Research Institute, ⁵Division of Paediatrics, Hospital for Sick Children, Toronto, Canada, ⁶Department of Neurology, West China Hospital, Sichuan University, Chengdu, Sichuan 610041, China, ⁷Department of Radiology, ⁸Department of Neurology, Massachusetts General Hospital, Boston, Massachusetts 02115, ⁹Department of Medicine, Center for Immunology and Inflammatory Diseases, Massachusetts General Hospital, Harvard Medical School, Boston, Massachusetts 02114, and ¹⁰Department of Biomedical Engineering, Tufts University, Medford, Massachusetts 02155

Repetitive mild traumatic brain injury (mTBI) in children and adolescents leads to acute and chronic neurologic sequelae and is linked to later life neurodegenerative disease. However, the biological mechanisms connecting early life mTBI to neurodegeneration remain unknown. Using an adolescent mouse repetitive closed head injury model that induces progressive cognitive impairment in males and anxiety in females in the absence of overt histopathology, we examined transcriptional and translational changes in neurons isolated from sham and injured brain in the chronic phase after injury. At 14 months, single-nuclei RNA sequencing of cortical brain tissue identified disruption of genes associated with neuronal proteostasis and evidence for disrupted ligand-receptor signaling networks in injured mice. Western blot analysis of isolated neurons showed evidence of inflammasome activation and downstream IL-1 β processing, as previously demonstrated in acute CNS injury models, and accumulation of misfolded, hyperphosphorylated tau, and changes in expression of proteins suggestive of impaired translation in males but not in females. At 6 months, injured IL-1 receptor 1 (*IL-1R1*) KO mice, which are protected from postinjury cognitive deficits, had decreased accumulation of pro-IL-1 β and misfolded tau in cortex and cerebellum, suggesting that IL-1R1 is upstream of inflammasome priming (defined as increase in pro-IL-1 β) and abnormal tau phosphorylation. Together, our findings provide evidence for neuronal inflammasome activation and impaired proteostasis as key mechanisms linking repetitive mTBI in adolescence to later life neurologic dysfunction and neurodegeneration.

Key words: adolescent; closed head injury; inflammasome; neuroinflammation; proteostasis; tauopathy

Significance Statement

Repetitive mild closed head injury in adolescent male mice leads to impaired proteostasis, tau phosphorylation, and inflammasome activation in neurons later in adulthood through mechanisms involving IL-1 receptor 1. The data are the first to link repetitive mild traumatic brain injury in adolescence to neurodegeneration and suggest molecular targets and pathways to prevent neurologic sequelae in the chronic period after injuries.

Received Mar. 31, 2021; revised Oct. 6, 2021; accepted Dec. 6, 2021.

Author contributions: L.W., B.T.K., and M.J.W. designed research; L.W., B.T.K., B.F., T.C., G.J., T.Y., E.S. Levy, E.S. LaRovere, J.Y.C., and A.B.-W. performed research; L.W., B.K., B.F., and B.K. analyzed data; L.W. wrote the first draft of the paper; B.K., E.H.L., J.E., and D.L.K. edited the paper; M.J.W. wrote the paper.

This work was supported by National Institutes of Health/National Institute of Neurological Disorders and Stroke R01NS096550 to M.J.W., K08 NS112338-02 to B.T.K., RF1AG051506 and R01AI119065 to J.E.K., and R01NS092847-01 to D.L.K.

The authors declare no competing financial interests.

Correspondence should be addressed to Michael J. Whalen at mwhalen@mgh.harvard.edu.

<https://doi.org/10.1523/JNEUROSCI.0682-21.2021>

Copyright © 2022 the authors

Introduction

Between 2 million and 3.8 million cases of mild traumatic brain injury (mTBI), or concussion (defined as symptomatic mTBI without structural brain damage on routine imaging), are estimated to occur each year in the United States (Langlois et al., 2006; Centers for Disease Control and Prevention, 2011, 2017; McCrory et al., 2013). Children and adolescents account for over half of sports-related concussions (Faul et al., 2010; Choe et al., 2012), and epidemiological studies suggest that the incidence of

adolescent concussion in the general population is increasing (Marin et al., 2014; Zhang et al., 2016). Recent data estimate the incidence of all TBI in children and adolescents at ~1 million cases per year, with most of these cases being mTBI (Taylor et al., 2017). A growing body of evidence suggests a greater risk of neurologic sequelae when mTBI occurs while the brain is still developing (Field et al., 2003; Giza and Prins, 2006; Hessen et al., 2007; Levin et al., 2007; Yeates, 2010; Baillargeon et al., 2012; Yeates et al., 2012; Zuckerman et al., 2012; Harmon et al., 2013; Kriz et al., 2017). Up to 30% of children and adolescents may suffer from prolonged, debilitating postconcussion symptoms after even a single mTBI (Barlow et al., 2010; Yeates, 2010; Yeates et al., 2012; Barlow, 2016; Zemek et al., 2016). While avoiding athletics until clinical symptoms resolve is currently the mainstay of therapy (Halstead et al., 2010), whether or not this strategy prevents later neurologic sequelae of mTBI is unknown.

Growing awareness of the potential dangers of repeated mTBI during childhood and adolescence has resulted in rule changes in youth sports designed to limit the number of head impacts and hence the likelihood of developing neurodegenerative disease later in life. Epidemiological evidence links moderate and severe TBI to later development of neurodegenerative disease, such as Alzheimer's disease (AD), Parkinson's disease, amyotrophic lateral sclerosis, and cognitive dysfunction (Smith et al., 2013; Gardner and Yaffe, 2015; Rabinowitz et al., 2015), whereas repetitive mTBI in adults is associated with development of chronic traumatic encephalopathy (CTE), a neurodegenerative disease with unique histopathological features (McKee, 2020). Some epidemiological studies have shown associations between playing contact sports earlier in childhood with increased risk of dementia and other neurologic sequelae later in life (Stamm et al., 2015a,b; Alosco et al., 2018; Schultz et al., 2018), while others have not (Solomon et al., 2016; Deshpande et al., 2017). Pathologic studies have shown changes consistent with CTE in the brains of adult (McKee et al., 2013) and even some adolescent football players (Tagge et al., 2018). However, the clinical studies are affected by case selection bias and an unknown incidence of CTE in the general population; hence, interpretation of the data is controversial (Smith et al., 2013; Mez et al., 2017; Binney and Bachynski, 2019; Casper et al., 2019; Stewart et al., 2019). Despite careful pathologic studies of brains of athletes and soldiers with CTE (McKee, 2020), the exact cellular and molecular mechanisms linking repetitive mTBI to neurodegeneration remain poorly defined, in part because the relevant animal models often fail to develop key histopathological features of human CTE (Gangolli et al., 2019; Mouzon et al., 2019; Bachstetter et al., 2020). Moreover, very few studies have examined long-term sequelae of mTBI in adolescent mTBI models, with one study showing increased brain amyloid β deposition at 1 year after repetitive mTBI in adolescent rats expressing human mutant APP/PS1 transgenes (Grant et al., 2018; Wu et al., 2019). To date, mechanistic studies examining the chronic stages of repetitive mTBI in WT adolescent animal models are lacking (Wu et al., 2019).

To address this gap, we modified an adolescent mouse repetitive closed head injury (CHI) model (Wu et al., 2019) to develop progressive learning and memory deficits and used single-nuclei RNA sequencing (snRNA-seq) to identify changes in putative molecular pathways associated with neurodegeneration. We identified disruption of gene expression associated with protein homeostasis (proteostasis), and evidence for mTOR pathway activation, accumulation of hyperphosphorylated and misfolded Tau, NLRP1 inflammasome activation and processing of IL-1 β , the primary substrate of activated inflammasomes, at the protein

level in neurons from injured male mice at 14 months after injuries. In brain tissue, microgliosis and accumulation of phosphorylated Tau were prevented by IL-1 receptor 1 (IL-1R1) KO. These data provide direct evidence for mechanisms by which repetitive mTBI in adolescence might lead to subsequent development of dementia and neurodegenerative disease later in life.

Materials and Methods

Mice. Adolescent (day of life [DOL] 38) male C57/BL6 mice and IL1 receptor 1 knock out (*IL1R1*^{-/-}) mice (The Jackson Laboratory) were used for experiments. Mice were housed for 12 h day/night cycles in laminar flow racks in a temperature-controlled room. Food and water were given *ad libitum*. All procedures were approved by the Massachusetts General Hospital Institutional Animal Care and Use Committee and performed in accordance with the National Institutes of Health's *Guide for the care and use of laboratory animals*. Studies were performed according to ARRIVE guidelines, and data were obtained by investigators blinded to study groups.

CHI model. The CHI model was used as previously described with minor modifications (Khuman et al., 2011). Mice were anesthetized with 2.5% isoflurane (Anaquest) for 90 s in a 70% N₂O/30% O₂ Fluotec 3 vaporizer (Colonial Medical). Mice were placed on a Kimwipe (Kimberly-Clark) and grasped by the tail, and the head was positioned under a hollow tube (diameter 10 mm). A lead cylindrical weight (54 g) was dropped 46 inches onto the dorsal aspect of the skull directly above the right (day 1, 3) or left (day 2) ear between the coronal and lambdoid sutures. The head readily penetrated the Kimwipe following impact in the anterior-posterior plane. Sham injured mice were subjected to anesthesia without weight drop. Injured mice were recovered in room air in their cages. Three-hit (3HD) mice were injured once daily for 3 consecutive days to model repetitive mTBI that might occur over the span of adolescence in humans, which lasts for 2 weeks in mice (Flurkey et al., 2007). One-hit (1HD) mice were injured once for the first day and subjected to anesthesia without weight drop for the following 2 d. Latency to spontaneous righting from a supine position was recorded for all mice on day 1.

Morris Water Maze (MWM). On each day of testing, mice were acclimatized to the room for at least 30 min. Mice were tested in a MWM task 3 weeks (males) or 3 months (females) after the last injury and again in a reverse MWM paradigm at 6 and 12 months. The MWM was performed as previously described with minor modifications (Mannix et al., 2013). Each mouse was subjected to 7 hidden platform trials (1 or 2 trials per day). Probe trials were performed 24 h after the last hidden platform trial by allowing the mice to swim for 30 s with the platform removed and recording the time spent in the target quadrant. For each reverse MWM, the platform location was moved to a unique quadrant and mice were subjected to 4–7 hidden platform trials (1 or 2 trials per day), followed by probe trials.

Rotarod. At 1, 6, and 12 months after injury, mice were subjected to rotarod testing. Mice were tested for 3 d with three trials per day on an accelerating rod (0–40 revolutions per minute over 200 s). Time on the rotarod and maximum speed attained before falling were recorded for each mouse.

Elevated plus maze. Elevated plus maze testing was performed at 3 (females only), 6, and 12 months after injury. The 24-inch-high apparatus consisted of two 52 inch \times 3 inch platforms with a 3 inch \times 3 inch square area at their intersection. The closed arms of the platform had walls 4 inches high, whereas the open arms had none. Each mouse was placed in the central square and video-recorded for 5 min. The apparatus was cleaned with 70% ethanol between trials. Video recordings were analyzed by Any Maze software for mean speed and percent time in closed and open arms.

Open field test. At 1 year after injury, mice were placed in separate cages secured with metal wiring tops and movements were video-recorded for 6 h. Any Maze software was used to assess mean speed and distance traveled.

Porsolt forced swim test. Forced swim tests were performed at 6 months or 1 year after injury. The apparatus consisted of a 4 L glass beaker filled with 2 L of water (25°C). Mice were placed in the water for 5 min, and swimming movements were recorded by the Photograph

Booth program. Latency to freezing/immobility and total freezing time were experimental endpoints.

Sucrose preference test. The sucrose preference test was performed in female mice at 1 year after injury based on a two-bottle choice paradigm (Liu et al., 2018). The whole test, including adaptation, baseline measurement, and testing, was performed over 8 d. Sucrose preference was calculated as (sucrose water intake/total water intake) \times 100%.

Isolation of brain cells by magnetic beads. Mice were transcardially perfused with PBS, and the brain was removed, digested using a Neural tissue dissociation kit (Roche Diagnostic), and mechanically dissociated with a plastic pipette. After centrifugation at $1000 \times g$ (7 min), the cell pellet was resuspended and incubated with myelin removal beads (Miltenyi Biotec) for 40 min on ice. After washing in PBS, Dynabeads (Thermo Fisher Scientific) conjugated to anti-CD31 (BD Pharmingen) or anti-CD11b (Biolegend) were added and a magnetic separator was used to recover the bead-bound cells. Unbound cells were incubated with anti-ACSA⁺ beads (Miltenyi Biotec) and separated using LS columns (Miltenyi Biotec). Neurons were isolated using a neuron isolation kit (Miltenyi Biotec). Isolated cells were frozen at -80°C until processing for Western blot. The purity of neurons was confirmed by lack of reactivity with antibodies against astrocyte, microglia, endothelial, and pericyte markers.

Western blot. Isolated brain cells were lysed in 1% Triton X-100 lysis buffer (150 mM NaCl, 20 mM Tris-Cl, pH 7.5, 1% Triton X-100, 1 mM EDTA, 3 mM NaF, 1 mM B-glycerophosphate, 1 mM sodium orthovanadate, 5 μM idacetamide [cysteine protease inhibitor], 2 μM N-ethylmaleimide [cysteine protease inhibitor], phosphatase and protease inhibitor cocktails [Thermo Fisher Scientific]). After sonication, samples were centrifuged at $1000 \times g$ for 10 min to precipitate the nuclear fraction, and the supernatant was transferred to a new tube and spun at $20,000 \times g$ for 30 min at 4°C . Supernatants were collected and diluted in 4 \times Laemmli buffer to prepare soluble fractions for Western blot analysis. Pellets (insoluble fraction) were washed once in a fresh aliquot of lysis buffer and spun at $20,000 \times g$ for 15 min. Following wash, the supernatant was discarded and pellets were dissolved in lysis buffer containing 8 M urea. Samples were then added to 4 \times Laemmli buffer. Both Triton-soluble fractions and urea-soluble fractions were subjected to Western blotting as previously described (Khuman et al., 2011). Membranes were incubated overnight at 4°C with the following primary antibodies: anti- β -actin antibody (1:10,000, Cell Signaling Technology), anti-AT8 (1:1000, Sigma), anti-tau5 (1:1000, Invitrogen), anti-IL1b (1:1000, Abcam), anti-caspase1 (1:1000, Novus), anti-NLRP3 (1:1000, Cell Signaling Technology), anti-NLRP1 (1:1000, Invitrogen), and anti-CP13, anti-MC1, anti-PHF1, and anti-RZ3 (kind gifts from the late Peter Davies, Feinstein Institute, Manhasset, NY). After incubation with peroxidase-conjugated secondary antibodies (1:5000, Cell Signaling Technology), visualization was enhanced by ECL (EMD Millipore) detection. The results were normalized to β -actin. Optical density was assessed using ImageJ software.

Immunohistochemistry for phospho-tau and β amyloid proteins. Mice were transcardially perfused with PBS, and brains were postfixed in 4% PFA for 48 h, cryoprotected in 15% for 24 h, and then 30% sucrose, frozen at -80°C and cut on a cryostat at 12 μm .

AT8 and amyloid β immunohistochemistry. PFA-fixed brain sections were washed twice with DPBS (without calcium and magnesium) before undergoing fixation with 95% ethanol (precooled to 4°C) for 10 min. Antigen retrieval was performed with a 15 min incubation of prewarmed (37°C) trypsin (0.25%) before blocking endogenous peroxidase activity with a 10 min incubation in Bloxall endogenous peroxidase and alkaline phosphatase blocking solution (Vector Laboratories, SP-6000-100). Sections were blocked in Mouse-on-Mouse IgG Blocking Reagent (Mouse-on-Mouse Detection Kit, Vector Laboratories, BMK-2202) for 1 h, followed by a 5 min incubation in Mouse-on-Mouse kit diluent. Sections were incubated with primary anti-AT8 (Invitrogen 1:250) antibody and anti-amyloid β antibody (Millipore, 1:400) in Mouse-on-Mouse kit diluent (Vector MOM Kit) for 30 min, before being visualized with the avidin-biotin HRP technique in accordance with the manufacturer's instructions. Sections were then mounted with Vectamount Permanent Mounting Medium (Vector Laboratories, H-

5000). Brightfield images were subsequently obtained using Nikon Microscope; 200-d-old APP/PS1 double-transgenic mice expressing a chimeric mouse/human amyloid precursor protein (Mo/HuAPP695swe) and a mutant human presenilin 1 (PS1-dE9) mice brain sections were stained together as a positive control for the methods.

MC1 immunohistochemistry. PFA-fixed brain sections were washed 4 times for 5 min each in TBS with 0.25% Triton X-100 before quenching endogenous peroxidase activity with 0.3% H_2O_2 diluted in 90% methanol for 30 min. Sections were then blocked in 5% milk diluted in TBS for 1 h before incubating in the primary antibody of paired helical filaments overnight (MC1, 1:100, diluted in TBS with 5% milk) at 4°C . The following day, sections were washed 4 times for 5 min each in TBS with 0.05% Triton X-100, and then incubated with secondary antibody (goat anti-mouse IgG1 1:1000) in 20% superblock with 0.05% Triton X-100 in TBS for 2 h at room temperature. Four more washes were performed followed by an hour-long room temperature incubation in streptavidin HRP (1:1000) diluted in TBS with 0.05% Triton X-100 and 20% Superblock. After three TBS washes, the primary antibody was visualized with DAB according to the manufacturer's instructions (Vector Laboratories, SK-4100). MC1 Tau antibodies and protocols were generously provided by Peter Davies (Feinstein Institute for Medical Research, Bronx, NY); 200-d-old APP/PS1 double-transgenic mice brain sections were used as a positive control for the staining methods.

IBA1 immunofluorescence staining. PFA-fixed brain sections were washed 3 times with DPBS (without calcium and magnesium) before incubation in DPBS with 10% normal goat serum for 15 min. DPBS with 10% normal goat serum was used for overnight primary antibody incubation with IBA1 (Wako, 1:500) at 4°C . The following day, brain sections were washed 3 times before a 90 min incubation at room temperature with anti-rabbit IgG-Cy3 conjugated secondary antibody (1:300; Jackson ImmunoResearch Laboratories). Slides were analyzed using a Nikon Eclipse Ti-S fluorescence microscope (Micro Video Instrument) using the appropriate excitation/emission spectra. Sections were analyzed by a blinded investigator using ImageJ software (National Institutes of Health). Brain regions assessed were $\times 200$ microscopic fields ($1100 \times 1100 \mu\text{m}$) in cortex ($n = 2$ fields/section, four sections per mouse = 8 fields/mouse), CA1 (12 fields in 4 sections per mouse), dentate gyrus (12 fields in 4 sections per mouse), striatum (16 fields in 4 sections/mouse), and cerebellum (16 fields in 4 sections/mouse). Cell count data for each mouse were the average of the total brain fields counted.

Single-nuclei RNA sequencing. Frozen brain tissue was thawed in 500 μl buffer HB (0.25 M sucrose, 25 mM KCl, 5 mM MgCl_2 , 20 mM Tricine-KOH, pH 7.8, 0.15 mM spermine tetrahydrochloride, 0.5 mM spermidine trihydrochloride, 1 mM DTT). The tissue was transferred to a 2 ml Dounce homogenizer; 500 μl 5% IGE PAL CA-630 (Sigma) and 1 ml HB were added to the tissue, and the tissue was homogenized with a tight pestle 10–15 times. The sample was transferred to a 15 ml tube and total solution brought to 9 ml with HB. In a Corex tube (Thermo Fisher Scientific), 1 ml 30% iodixanol was layered on top of 1 ml 40% iodixanol. The 9 ml sample was layered on top of the iodixanol cushion. The sample was spun at $10,000 \times g$ for 18 min; 1 ml of sample at the 30%–40% iodixanol interface was collected. After counting nuclei with a hemocytometer, the sample was diluted to 100,000 nuclei/ml with 30% iodixanol (with Rnasin) and subjected to single nuclear droplet encapsulation with inDrops.

Individual nuclei were captured and barcoded using the inDrops platform as previously described (Kalish et al., 2021). Briefly, single-cell suspensions were fed into a microfluidic device that packaged the cells with barcoded hydrogel microspheres and reverse transcriptase/lysis reagents. After cell encapsulation, primers were photo-released by UV exposure. Two libraries of ~ 3000 cells each were collected for each sample. Indexed libraries were pooled and sequenced on a Nextseq 500 (Illumina).

Sequencing data analysis. Sequencing data were aligned to the genome and processed according to a previously published pipeline (<https://github.com/indrops/indrops>). Briefly, this pipeline was used to build a custom transcriptome from Ensembl GRCm38 genome and GRCm38.84 annotation using Bowtie 1.1.1, after filtering the annotation gtf file (gencode.v17.annotation.gtf filtered for feature_type = "gene," gene_type = "protein_coding" and gene_status = "KNOWN"). Unique molecular identifiers (UMIs) were used to link sequence reads back to

individual captured molecules. All steps of the pipeline were run using default parameters unless explicitly stated.

Quality control, dimensionality reduction, and clustering of cells. All cells were combined into a single dataset. All mitochondrial genes were removed from the dataset. Cells with <500 or >15,000 UMI counts were excluded. Cells were then clustered using the Seurat R package. The data were log-normalized and scaled to 10,000 transcripts per cell. Variable genes were identified using the following parameters: x_{low} .Cutoff = 0.0125, x_{high} .Cutoff = 3, y .Cutoff = 0.5. We limited the analysis to the top 30 principal components. Clustering resolution was set to 0.6. Clusters containing <100 cells were discarded. The Seurat FindMarkers function was used to identify genetic markers of cellular subtypes. The expression of known marker genes was used to assign each cluster to one of the main cell types. Doublets were removed using Scrublet. Clusters from each cell type were combined and the Seurat-based clustering repeated to characterize subtype diversity.

Identification of differentially expressed genes. To identify differentially expressed genes by cell type, we performed a differential gene expression analysis using Monocle2. The analysis was conducted on each cell type, comparing sham and 3HD samples. The data were modeled and normalized using a negative binomial distribution. Genes whose false discovery rate (FDR) was <5% were considered statistically significant. Receptor-ligand analysis was performed using CellChat (version 1.1.3).

Statistical analyses. Data are mean \pm SEM. All data with $n=5$ or more per group passed normality tests (Anderson-Darling test and others). Data with $n=4$ /group (densitometry) were expected to be normally distributed. Data were analyzed using GraphPad Prism VII. MWM hidden and visible platform trials, and rotarod data were analyzed by two-factor repeated-measures ANOVA (group \times time). Other data were analyzed by unpaired t test or one-way ANOVA depending on the number of groups. Significance was set at $p < 0.05$.

Data and software availability. The raw reads of the sequencing data are submitted to NCBI-GEO. The accession is GSE167942.

Results

We induced mild repetitive CHI in anesthetized male and female adolescent (DOL 38) mice with a weight drop apparatus (54 g, 46 inch) as previously described (Wu et al., 2019). Mice were injured once and anesthetized for 3 consecutive days (1HD), injured once per day for 3 consecutive days (3HD), or subjected to anesthesia only for 3 days (sham). A total of 150 mice were used in the studies. None of the mice examined exhibited skull fractures, contusion, or intraparenchymal brain hemorrhage. On DOL 38 and at 1 year, body weight in sham and injured mice was not different in both males (Fig. 1A) and females (Fig. 2A); however, sham and 3HD females weighed significantly less than males at DOL 38 ($p < 0.0001$, t test; Figs. 1A, 2A). Following the first CHI, time to righting reflex was significantly increased in injured mice versus sham both in males (93 ± 15.3 s vs 16 ± 0.78 s, $p < 0.001$, $n=19$ or 20/group; Fig. 1B) and in females (63 ± 52.8 s vs 12.8 ± 2.8 s, $p < 0.001$, $n=18$ /group; Fig. 2B); however, time to righting reflex did not differ between injured males and injured females ($p=0.14$).

Emergence of behavioral deficits after repetitive CHI

We used a battery of behavioral tests to examine the effects of repetitive CHI on short- and long-term cognitive and motor outcome. In the rotarod, a test of striatal-dependent motor learning, 3HD males performed significantly worse versus sham at 3 weeks and 6 months but did not differ from sham at 1 year after injuries (Fig. 1C). 1HD and shams did not differ in rotarod performance at any time point examined (Fig. 1C).

In MWM tests, male 3HD mice and sham had similar performance in hidden platform trials at 3 weeks and reversal trials

at 1 month but were impaired in reversal trials versus sham at 6 months and 1 year, with no differences in swim speed at any time point examined (Fig. 1D,E). Male 3HD mice performed worse than sham in probe trials at 1 year (Fig. 1F). Male 1HD mice performed similarly in hidden platform and reversal trials versus sham, were worse in probe trials at 3 weeks, and had similar probe trial performance versus sham at 1, 6, and 12 months (Fig. 1D–F).

In the elevated plus maze, male injured and sham groups did not differ in percent time spent in the open arms at 6 months or 1 year (Fig. 1G). In the forced swim test, percent time immobile at 1 year was significantly less in 3HD versus sham but similar between 1HD and sham (Fig. 1H). In the overnight open field test, 3HD mice and 1HD mice did not differ from sham at 1 year (Fig. 1I).

To examine possible sex differences in neurologic outcome, we subjected female mice at DOL 38 to sham or 3HD and observed their behavior for up to 1 year. In the rotarod, 3HD females performed significantly worse than sham at 6 months and 1 year but did not differ from sham at 3 months after injuries (Fig. 2C). MWM performance in female 3HD was similar to sham at all time points tested for up to 1 year, except that female 3HD had increased time in the target quadrant in probe trials at 3 months (Fig. 2D–F). In an elevated plus maze, female 3HD mice spent significantly less time in the open arm compared with sham at 3 and 6, but not 12 months after injury (Fig. 2G). In a forced swim test, 3HD female mice spent more time freezing compared with sham at 1 year (Fig. 2H); however, female shams and 3HD had similar preference for sucrose in their drinking water (Fig. 2I), suggesting that motor or motivational deficits might underlie differences in the forced swim test. Female 3HD also performed similar to sham in the open field and novel object recognition test (performed to validate the females' lack of a phenotype in the MWM) at 1 year (Fig. 2J,K). Because female sham and 3HD groups did not differ with respect to cognitive deficits, the primary behavioral outcome of the study, we focused the RNA sequencing analyses on male mice.

snRNA-seq implicates chronic impairment of proteostasis after 3HD in male adolescent mice

To characterize cell type-specific mechanisms related to impaired cognition and motor function in the adolescent mouse 3HD model, we performed snRNA-seq on cortical brain tissue specimens from male sham and 3HD mice. Nuclei were isolated from frozen parietal cortex tissue and were subjected to single-nuclei capture and mRNA barcoding using the inDrops platform (Klein et al., 2015). After quality control filtering, the dataset of 3HD and sham samples contained 34,765 nuclei, detecting on average 2125 transcripts (UMIs) and 1895 genes per nucleus (for quality control metrics, see Extended Data Fig. 3-1A,B). We identified 18 transcriptionally distinct clusters (Fig. 3A), and we used canonical marker genes to classify nuclei into eight main cell types: excitatory neurons (*Slc17a7+*), interneurons (*Gad2+*), claustrum (*Nr4a2+*), oligodendrocytes (*Olig1+*), oligodendrocyte precursors (*Pdgfra+*), astrocytes (*Gjal1+*), endothelial cells (*Cldn5+*), and striatum (*Gpr88+*) (Fig. 3B). There were no differences in the distribution of major cell types between conditions. To further capture cellular diversity, we subjected major cell types to a second iteration of principal component analysis and subclustering. In doing so, we identified nine layer-specific excitatory subpopulations (Extended Data Fig. 3-1C), as well as distinct parvalbumin-, somatostatin-, SST-, and Npy-positive interneurons (Extended Data Fig. 3-1D).

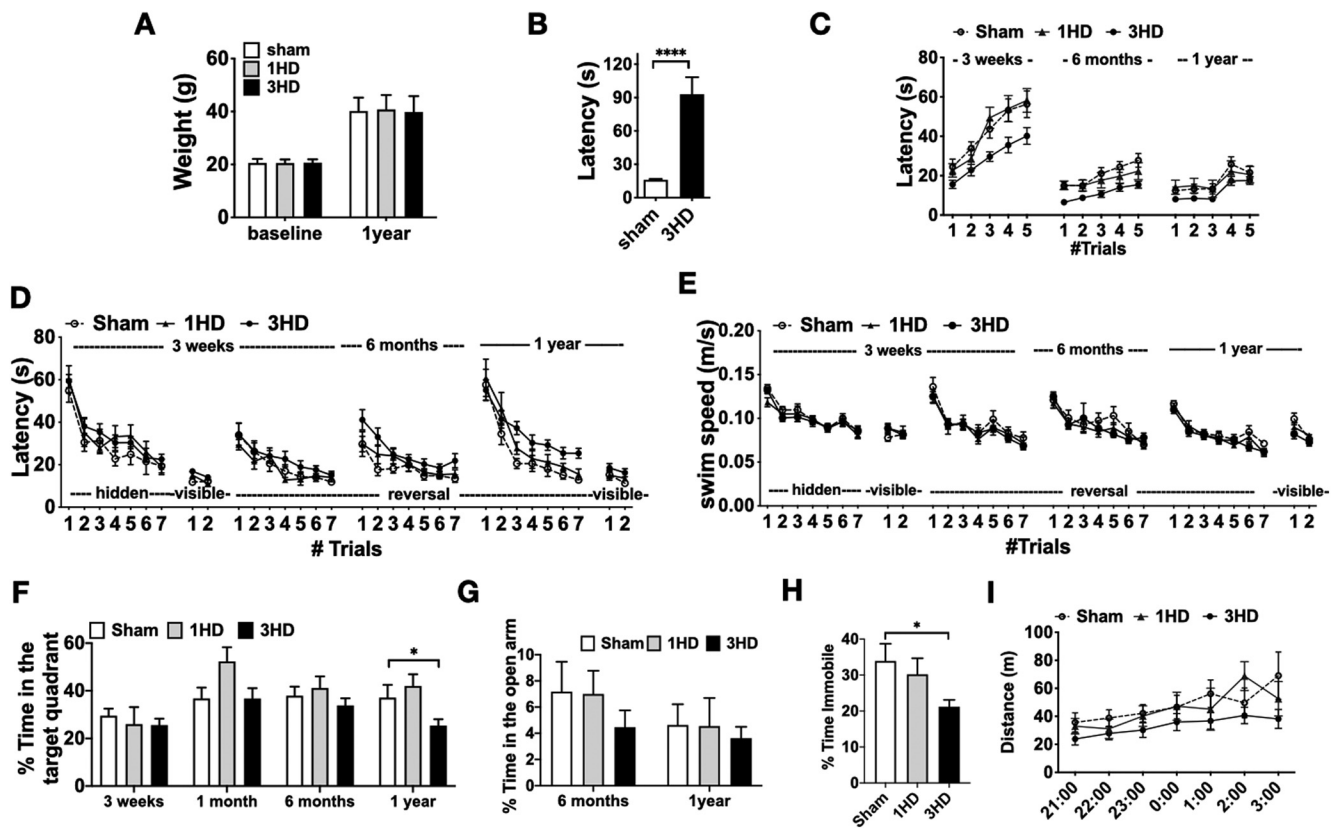


Figure 1. Physiologic and behavioral sequelae of three daily closed head injuries (3HD) in male mice. **A**, Body weight before and 1 year after sham and 3HD (one-way ANOVA, Tukey's test, $n = 10$ – 19 /group). **B**, Time to righting after the first CHI (3HD) or sham (unpaired t test, $n = 10$ – 20 /group, **** $p < 0.0001$). **C**, Rotarod test performance was worse in 3HD versus sham at 3 weeks (two-way repeated-measures ANOVA, $F_{(1,28)} = 12.06$, $p = 0.0017$ for group) and 6 months (two-way repeated-measures ANOVA, $F_{(1,28)} = 14.7$, $p = 0.0007$ for group) but not at 1 year (two-way repeated-measures ANOVA, $F_{(1,28)} = 4.092$, $p = 0.0527$ for group, $n = 11$ – 19 /group). Rotarod performance did not differ in 1HD versus sham at 3 weeks (two-way repeated-measures ANOVA, $F_{(1,19)} = 0.0028$, $p = 0.96$ for group), 6 months (two-way repeated-measures ANOVA, $F_{(1,19)} = 0.51$, $p = 0.48$ for group), or 1 year (two-way repeated-measures ANOVA, $F_{(1,18)} = 0.0036$, $p = 0.95$ for group, $n = 10$ or 11 /group). **D**, In MWM hidden platform performance, 3HD was similar to sham at 3 weeks (two-way repeated-measures ANOVA, $F_{(1,28)} = 1.84$, $p = 0.19$ for group) and 1 month (reversal trial, two-way repeated-measures ANOVA, $F_{(1,28)} = 0.7281$, $p = 0.40$ for group). However, 3HD performed worse in reversal trials than sham at 6 months (two-way repeated-measures ANOVA, $F_{(1,28)} = 6.67$, $p = 0.015$ for group) and 1 year (two-way repeated-measures ANOVA, $F_{(1,28)} = 11.50$, $p = 0.0021$ for group, $n = 11$ – 19 /group). Visible platform performance in 3HD differed from sham at 3 weeks (two-way repeated-measures ANOVA, $F_{(1,28)} = 6.85$, $p = 0.014$ for group), consistent with a striatal lesion, but not at 1 year (two-way repeated-measures ANOVA, $F_{(1,28)} = 2.45$, $p = 0.13$ for group). 1HD mice performed similarly to sham in hidden platform trials at 3 weeks (two-way repeated-measures ANOVA, $F_{(1,19)} = 0.79$, $p = 0.39$ for group), 6 months (two-way repeated-measures ANOVA, $F_{(1,19)} = 0.22$, $p = 0.65$ for group), 6 months (two-way repeated-measures ANOVA, $F_{(1,19)} = 1.12$, $p = 0.30$ for group), and 1 year (two-way repeated-measures ANOVA, $F_{(1,18)} = 1.97$, $p = 0.18$ for group, $n = 11$ – 20 /group). 1HD did not differ from sham in visible platform trials at 3 weeks (two-way repeated-measures ANOVA, $F_{(1,19)} = 0.81$, $p = 0.38$ for group) and 1 year (two-way repeated-measures ANOVA, $F_{(1,18)} = 0.26$, $p = 0.62$ for group, $n = 10$ or 11 /group). **E**, Swim speed did not differ among groups at any time point examined (two-way repeated-measures ANOVA, 3HD vs sham at 3 week hidden: $p = 0.38$ for group, 3 week visible: $p = 0.44$ for group, 1 month reversal: $p = 0.38$ for group, 6 months reversal: $p = 0.60$ for group, 1 year reversal: $p = 0.21$ for group, 1 year visible: $p = 0.16$ for group, $n = 11$ – 20 /group; 1HD versus sham at 3 week hidden: $p = 0.38$ for group, 3 week visible: $p = 0.33$ for group, 1 month reversal: $p = 0.58$ for group, 6 months reversal: $p = 0.49$ for group, 1 year reversal: $p = 0.40$ for group, 1 year visible: $p = 0.68$ for group, $n = 10$ – 11 /group). **F**, Percent time in the target quadrant was decreased in 3HD versus sham at 1 year ($p = 0.013$, one-way ANOVA, * $p = 0.038$, t test), but was not different among groups at 3 weeks ($p = 0.77$ one-way ANOVA), 1 month ($p = 0.07$ one-way ANOVA), or 6 months ($p = 0.37$ one-way ANOVA, $n = 11$ – 19 /group). **G**, In elevated plus maze, percent time spent in the open arm was not different in sham, 1HD, and 3HD groups at 6 months ($p = 0.42$, one-way ANOVA) and 1 year ($p = 0.83$, one-way ANOVA, $n = 10$ – 19 /group). **H**, Percent time swimming in a forced swim test was less in 3HD versus sham ($p = 0.02$ one-way ANOVA, * $p = 0.0073$ t test, $n = 11$ – 19 /group), but did not differ between 1HD and sham ($p = 0.59$ t test, $n = 9$ – 11 /group) at 1 year after injury. **I**, In the open field test, 3HD mice (two-way repeated-measures ANOVA, $F_{(1,28)} = 4.05$, $p = 0.054$ for group, $n = 10$ – 19 /group) and 1HD mice (two-way repeated-measures ANOVA, $F_{(1,19)} = 0.09$, $p = 0.77$ for group, $n = 10$ /group) did not differ from sham at 1 year.

We performed differential gene expression analysis within cell types to explore transcriptional signatures associated with 3HD. Genes with an FDR $< 5\%$ were considered statistically significant. We identified hundreds of differentially expressed genes (DEGs) across nearly all cell types with altered expression in the cortex of mice exposed to 3HD (Fig. 3C). All cell type-specific differential gene expression results are available in Extended Data Table 3-2. We used gene ontology analysis to broadly classify functional modules of genes that are significantly disrupted by repetitive CHI (all GO results in Extended Data Table 3-3).

In excitatory neurons, we found that DEGs were enriched for regulators of tau protein kinase activity, stress granule assembly, amyloid precursor protein biosynthesis, and cytoplasmic

translation (Fig. 3D). We identified increased expression of amyloid precursor protein (*App*) and Tripartite Motif Containing 32 (*Trim32*), and decreased expression of neprilysin (*Mme*) in excitatory neurons; these changes have been previously associated with neurodegeneration (Mohajeri et al., 2004; Farris et al., 2007) (Fig. 3E). Increased amyloid precursor protein expression is associated with increased β -amyloid peptide, which dampens excitatory synaptic transmission through both presynaptic and postsynaptic mechanisms (Ting et al., 2007). Additionally, *Trim32* encodes an E3 ubiquitin ligase that regulates oxidative stress-induced cell death and demonstrates increased expression in human AD (Yokota et al., 2006). *Neprilysin* (*Mme*), which was decreased in the chronic phase after 3HD, is a major amyloid

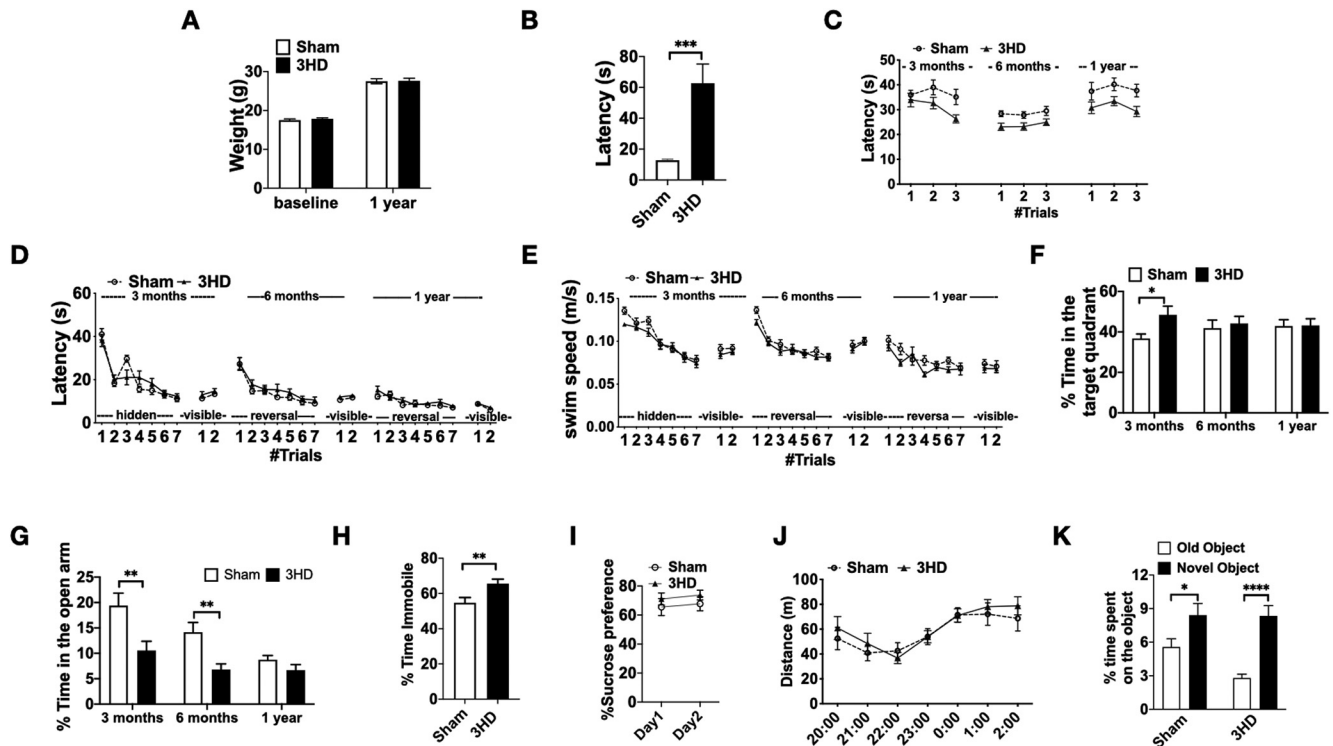


Figure 2. Physiologic and behavioral sequelae of 3HD in female mice. **A**, Body weight before and 1 year after sham and 3HD (baseline: $p = 0.41$; 1 year: $p = 0.92$, $n = 18/\text{group}$, t test). **B**, Time to righting after the first CHI (3HD) or first anesthetic (shams) ($***p = 0.0003$, $n = 18/\text{group}$, t test). **C**, Rotarod test performance was worse in 3HD versus sham at 6 months (two-way repeated-measures ANOVA, $F_{(1,34)} = 8.43$, $p = 0.0065$ for group) and 1 year (two-way repeated-measures ANOVA, $F_{(1,34)} = 5.23$, $p = 0.029$ for group) but not at 3 months (two-way repeated-measures ANOVA, $F_{(1,34)} = 3.77$, $p = 0.06$ for group) ($n = 18/\text{group}$). **D**, In the MWM, 3HD performed similar to sham in hidden platform trials at 3 months (two-way repeated-measures ANOVA, $F_{(1,34)} = 0.0045$, $p = 0.95$ for group), and in reversal trials at 6 months (two-way repeated-measures ANOVA, $F_{(1,34)} = 1.46$, $p = 0.23$) and 1 year (two-way repeated-measures ANOVA, $F_{(1,34)} = 1.03$, $p = 0.32$ for group). 3HD and sham did not differ in visible platform tests at 3 months (two-way repeated-measures ANOVA, $F_{(1,34)} = 1.38$, $p = 0.25$), 6 months (two-way repeated-measures ANOVA, $F_{(1,34)} = 1.67$, $p = 0.21$), and 1 year (two-way repeated-measures ANOVA, $F_{(1,34)} = 0.82$, $p = 0.37$ for group) ($n = 18/\text{group}$). **E**, Swim speed did not differ among groups at any time point examined (3HD vs sham at 3 months hidden: $p = 0.22$ for group, 3 months visible: $p = 0.31$ for group, 6 month reversal: $p = 0.20$ for group, 6 months visible: $p = 0.24$ for group, 1 year reversal $p = 0.18$, 1 year visible $p = 0.48$, $n = 18/\text{group}$, two-way repeated-measures ANOVA). **F**, In probe trials, 3HD performed better than sham at 3 months ($*p = 0.020$), and similar to sham at 6 months ($p = 0.67$) and 1 year ($p = 0.94$) ($n = 18/\text{group}$, t tests). **G**, In an elevated plus maze, 3HD spent significantly less time versus sham in the open arm at 3 months ($**p = 0.0066$) and 6 months ($**p = 0.0021$), but not at 1 year ($p = 0.14$) after injury ($n = 18/\text{group}$, t tests). **H**, In a forced swim test, 3HD spent more time immobile compared with sham at 1 year ($**p = 0.0082$) after injury ($n = 18/\text{group}$, t test). **I**, Sham and 3HD performed similarly in sucrose preference test at 1 year (two-way repeated-measures ANOVA, $F_{(1,34)} = 0.87$, $p = 0.36$, $n = 18/\text{group}$). **J**, In an open field test, segmented travel distance was not different between sham and 3HD at 1 year (two-way repeated-measures ANOVA, $F_{(1,33)} = 0.18$, $p = 0.68$ for group) ($n = 18/\text{group}$). **K**, In a novel object recognition test at 1 year, both sham ($*p = 0.033$) and 3HD ($****p = 0.000002$) groups spent more time on the novel object compared with the similar object at 24 h ($n = 18/\text{group}$, t test).

clearance enzyme and may also affect susceptibility to neurodegeneration after brain injury (Maetzler et al., 2010).

In interneurons, differentially expressed genes were enriched for mediators of lysosomal membrane organization, synaptic vesicle fusion, neurotransmitter transport, and cytoplasmic translation (Fig. 3F). Lysosome processing in particular is a critical component of proteostasis, and deficits in lysosome function are associated with neurodegenerative disease (Giovetti et al., 2020). 3HD was associated with decreased expression of the voltage-dependent potassium channel subunit Kv3.3 (*Kcnc3*); mutations in *Kcnc3* are associated with neurodevelopmental and neurodegenerative disorders (Nelson, 2006). 3HD was also associated with increased expression of *AChE*, which is responsible for terminating neurotransmission by rapid hydrolysis of acetylcholine. In AD, there is a loss of cholinergic neurons and an increase in the activity of *AChE* (Whitehouse et al., 1982; Apelt et al., 2002). Finally, we found a >50% decrease in expression of *Scyl2* in 3HD interneurons; *Scyl2* is a coated vesicle-associated kinase that suppresses excitotoxicity and promotes neuronal survival (Gingras et al., 2015) (Fig. 3G).

Interestingly, across both excitatory and inhibitory neurons, we found a widespread increase in the expression of numerous

ribosome subunit genes (e.g., *Rps29*, *Rps8*; Fig. 3E,G), which is also consistent with the DEG enrichment for regulators of mRNA translation. The expression of ribosome subunit genes is commonly upregulated in the aged brain (Ximerakis et al., 2019). Moreover, we identified mis-regulation of numerous eukaryotic translation initiation and elongation factors in excitatory (e.g., *Eif1*, *Eif2a*, *Eif3h*, *Eif4a1*, *Eif5a*, *Eif4a2*, *Eef1a1/2*, *Eef1g*) and inhibitory (*Eif4a1*, *Eif4g3*, *Eif4h*, *Eef1g*, *Eef1a1*) neurons (Fig. 3E, G). These factors are critical to mRNA translation, as they stabilize the formation of the ribosomal preinitiation complex or assist in the elongation of the nascent polypeptide chain. Protein synthesis and degradation defects are implicated in the pathogenesis of neurodegeneration; therefore, changes in genes that control ribosome biogenesis, the translational machinery, and stress granule assembly may contribute to chronic deficits after 3HD.

Non-neuronal cells, including astrocytes and oligodendrocytes, have been increasingly recognized for their role in the acute and chronic recovery from TBI, but their contribution to long-term neurologic dysfunction after mTBI is poorly understood. We found that expression of *Alcam*, a cell adhesion molecule, was increased >5-fold in 3HD astrocytes. We also identified increased expression of *Atp6v1h* and *S100a6* in 3HD astrocytes. *Atp6v1h* encodes a

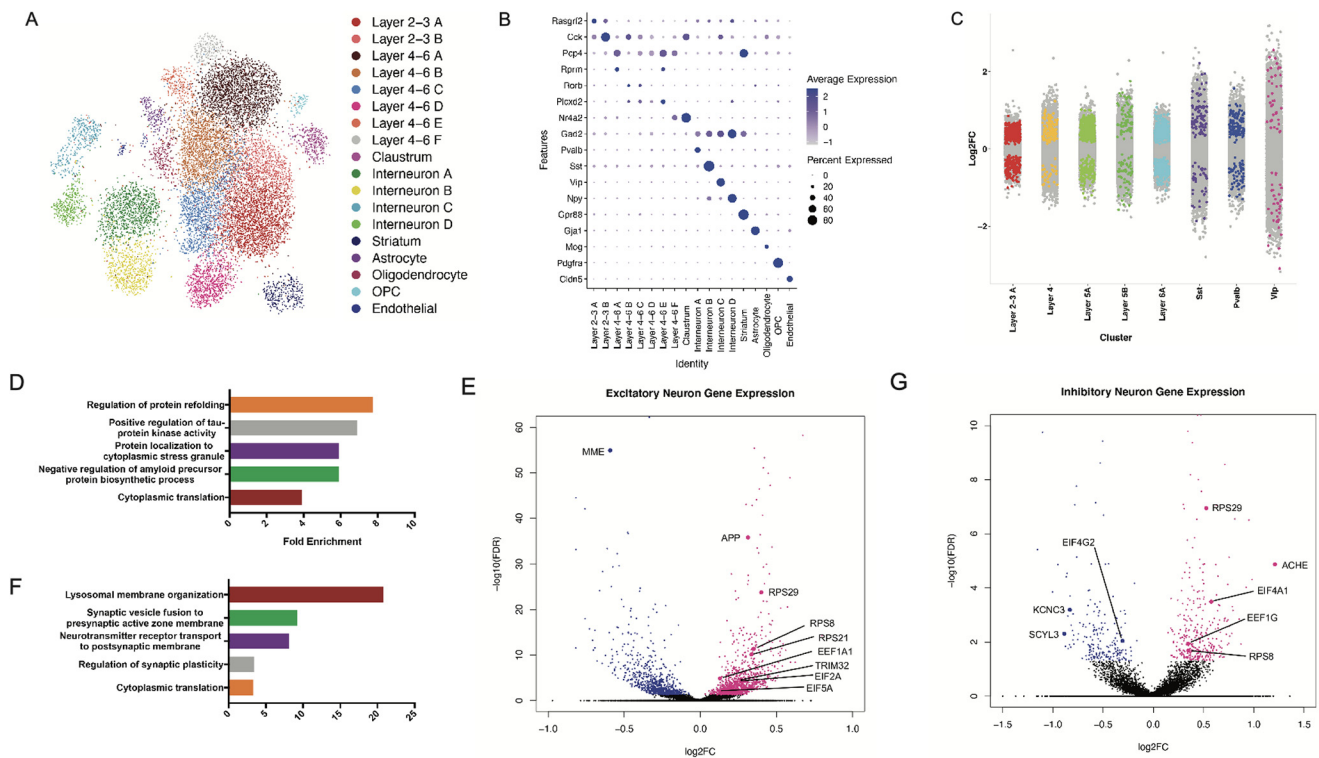


Figure 3. Single-cell sequencing of the adult mouse cortex 1 year following repetitive CHI in adolescent mice. **A**, Uniform manifold approximation and projection (UMAP) of all cells analyzed by snRNA-seq, with cell types labeled by color ($n = 18$ clusters). Data from $n = 3$ mice per group. **B**, Dot plot displaying marker gene expression across all cell types identified by scRNA-seq. Genes are displayed on the y axis, and cell types displayed on the x axis. Size of the dots indicates the percentage of cells within a cell type that express the gene. Color of the dot represents the expression level. **C**, Strip plot displaying differential gene expression between 3HD and sham conditions. Colored dots represent significant genes ($FDR < 0.05$). x axis displays select cortical cell types. Data from $n = 3$ mice per group. **D**, GO analysis of differentially expressed genes ($FDR < 0.05$) between 3HD and sham conditions in excitatory neurons. x axis displays fold enrichment relative to reference gene set. Data from $n = 3$ mice per group. **E**, Volcano plot of differential gene expression between 3HD and sham conditions in excitatory neurons. Colored dots represent statistical significance ($FDR < 0.05$). Positive \log_2FC (red dots) indicates higher gene expression in 3HD relative to sham. Negative \log_2FC (blue dots) indicates higher gene expression in sham relative to 3HD. Data from $n = 3$ mice per group. **F**, GO analysis of differentially expressed genes ($FDR < 0.05$) between 3HD and sham conditions in inhibitory neurons. x axis displays fold enrichment relative to reference gene set. Data from $n = 3$ mice per group. **G**, Volcano plot of differential gene expression between 3HD and sham conditions in inhibitory neurons. Colored dots represent statistical significance ($FDR < 0.05$). Positive \log_2FC (red dots) indicates higher gene expression in 3HD relative to sham. Negative \log_2FC (blue dots) indicates higher gene expression in sham relative to 3HD. Data from $n = 3$ mice per group.

protein subunit of a vacuolar ATPase involved in clathrin-mediated endocytosis (Geyer et al., 2002), and the role of *Atp6v1h* in regulating lysosomal pH has been linked to neurodegeneration (Colacurcio and Nixon, 2016). *S100a6* encodes an EF-hand calcium binding protein, and increased expression is consistent with astrocyte activation and astrogliosis. Elevated *S100a6* expression has been associated with numerous neurodegenerative disorders, including AD and amyotrophic lateral sclerosis (Hoyaux et al., 2002; Mori et al., 2010).

Together, snRNA-seq of the cortex at 14 months after 3HD revealed both cell type-specific and shared transcriptomic pathways mis-regulated by adolescent brain injury. In particular, we identified global disruption of genes that control protein homeostasis (proteostasis), including those that mediate mRNA translation, trafficking, and lysosomal degradation.

Disruption of ligand-receptor signaling networks after 3HD in adolescent mice

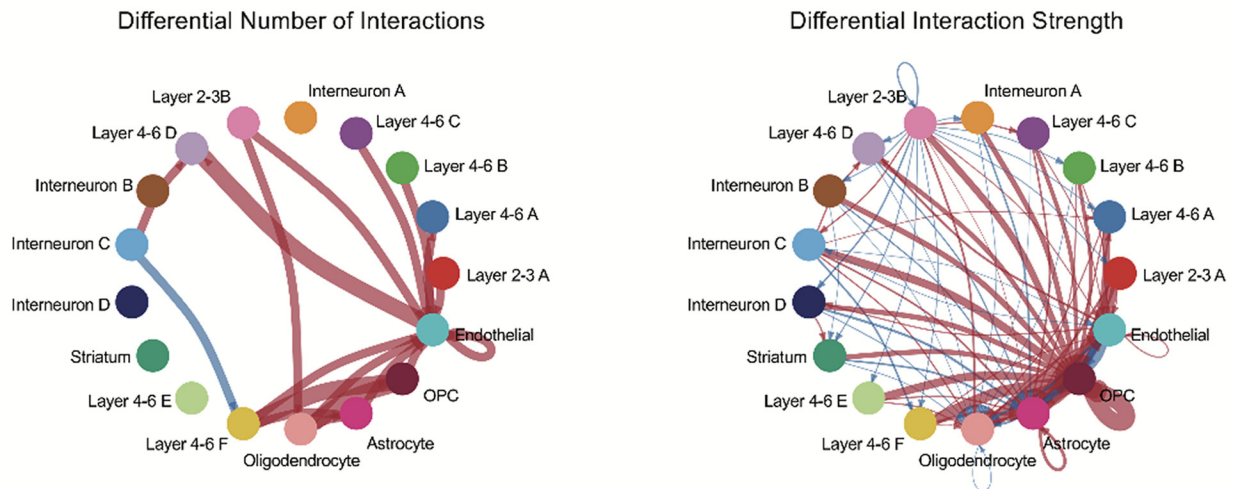
Multicellular coordination of cellular activity is essential for brain function, and the disruption in signaling homeostasis can have long-lasting consequences. Recent advances in single-cell sequencing analysis have enabled the systematic deconstruction of intercellular communication through detailed mapping of ligand-receptor pairs across cell types. Therefore, we used the R toolkit CellChat (Jin et al., 2021) to quantitatively map ligand-receptor networks in

our snRNA-seq data of the mouse cortex with the specific objective of identifying ligand-receptor networks perturbed by adolescent brain injury. We identified a significant shift in the number and strength of differential ligand-receptor interactions between the 3HD and sham conditions, particularly between endothelial, neuronal, and glial cell types (Fig. 4A). Most notably, *semaphorin* (*Sema3*) signaling was significantly increased in 3HD compared with sham (Fig. 4B). *Sema3c* expression was increased in endothelial cells after 3HD, while the expression of *Sema3* receptors *Plxnal1* and *Plxna2* was increased in layer 4–6 cortical neurons (Fig. 4C). The secreted *Sema3* proteins and their receptors neuropilins and plexins have long been studied for their role in repulsive axon guidance, but they are also critical for the immune response, remyelination, and revascularization after traumatic brain injury (Mecollari et al., 2014). Importantly, the related *Sema3* family member *Sema3a* has been recently shown to direct proteostasis through noncanonical modulation of the eIF2 α pathway and an increase in local translation (Cagnetta et al., 2019). This represents one signaling node with chronic perturbation after adolescent brain injury and a possible upstream mediator of long-term translational misregulation.

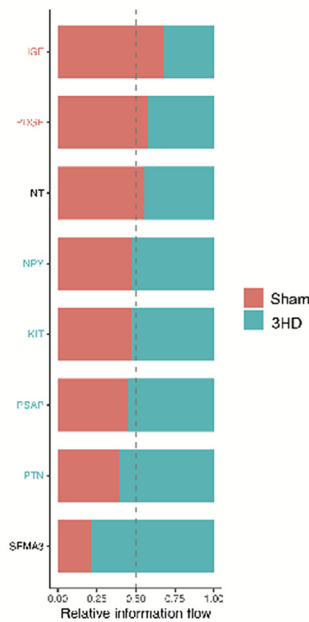
Activation of inflammasome proteins after 3HD in the brain of adolescent mice

One mechanism by which impaired proteostasis mediates neurodegeneration is through aberrant inflammasome activity (Plaza-

A



B



C

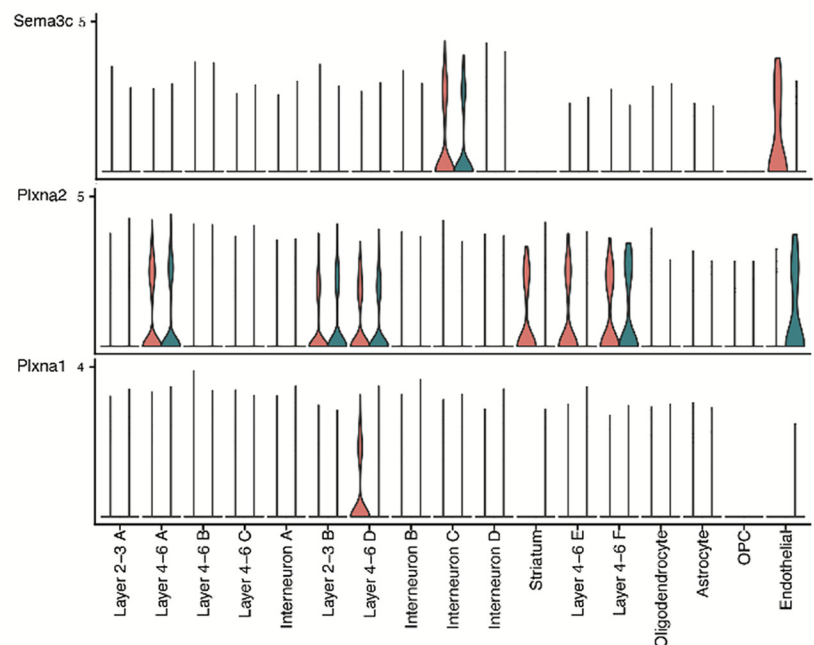


Figure 4. Receptor-ligand analysis of snRNA-seq after 3HD. **A**, Differential number (left) and strength (right) of receptor-ligand interactions across all cell types. Red lines indicate increased number or strength of interactions in 3HD versus sham. Blue lines indicate decreased number or strength of interactions in 3HD versus sham. **B**, Relative receptor-ligand signaling information flow, identifying pathways with shifts in predicted receptor-ligand interactions. **C**, Violin plots of genes involved in Sema3 signaling, across cell types (Sema3c, Plxna1, and Plxna2). Red indicates 3HD. Teal indicates sham condition.

Zabala et al., 2017; Sonninen et al., 2020). Inflammasomes are intracellular complexes composed of sensor (NLRP1, 3), adapter (ASC, AIM), and effector (caspase-1, 11) proteins that initiate IL-1 β and IL-18 processing and activation during an inflammatory response. Given our snRNA-seq data suggesting dysregulated proteostasis after adolescent brain injury, we hypothesized that 3HD would induce aberrant inflammasome activity in neurons in the chronic period after injuries. We previously reported cleavage of IL-1 β to its active fragment in cerebral endothelium at 11 d after 3HD in adolescent mice (Wu et al., 2019). To determine whether IL-1 β cleavage is dependent on inflammasome activation, we subjected WT and *caspase-1/11* double KO mice to sham and 3HD and used Western blot to detect IL-1 β in endothelial cells isolated by whole-brain immunopanning using CD31 magnetic beads at 11 d. As expected, processed IL-1 β was

detected in WT brain endothelium but not in endothelium of *caspase-1/11* double KO mice (Extended Data Fig. 5-1A), indicating that cleavage and activation of IL-1 β in brain endothelium that we previously reported after 3HD (Wu et al., 2019) are indeed dependent on inflammasome activity.

To examine IL-1 β processing in the chronic phase, we isolated CD31⁺ endothelial cells, CD11b⁺ leukocytes, CD13⁺ pericytes and neurons from brain at 14 months after sham and 3HD in males and isolated neurons in females using immunopanning. Western blot analyses showed increased cleavage of IL-1 β and caspase-1 and a significant increase in the full-length form of IL-1 β in neurons isolated from brains of male 3HD versus sham mice (Fig. 5A–E and Extended Data Fig. 5-2A), but IL-1 β processing in neurons did not differ between male 1HD and sham (Extended Data Fig. 5-1B,C), nor injured 3HD versus sham in

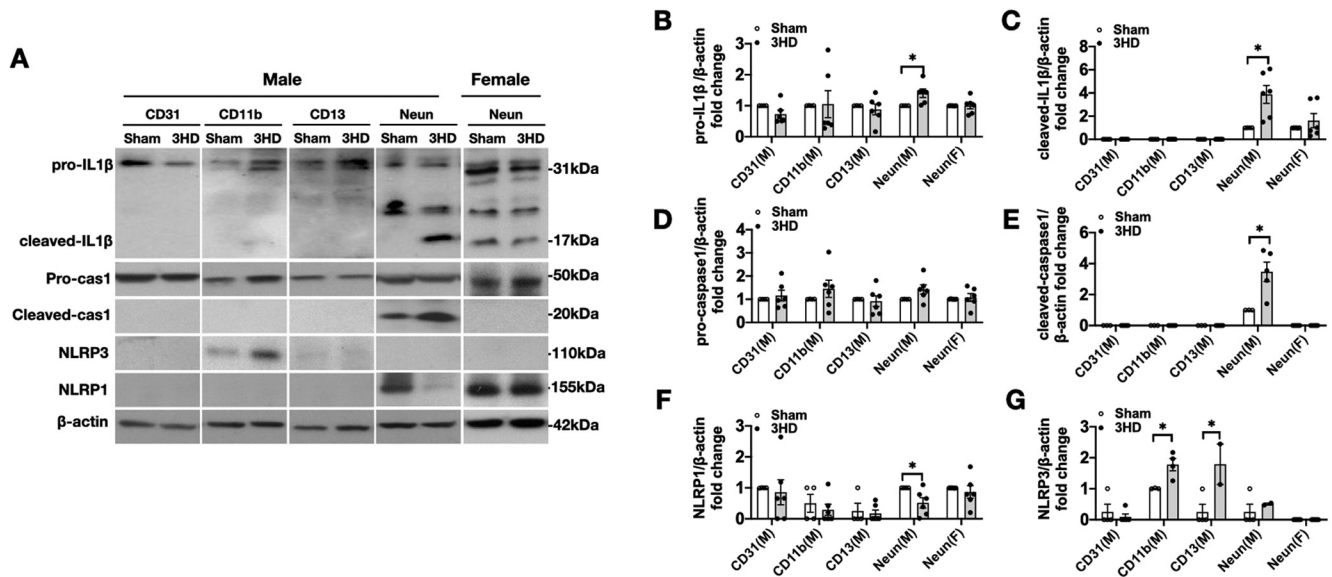


Figure 5. Evidence for cell-specific activation of inflammasome proteins after 3HD. **A**, Representative Western blot and (**B–G**) densitometry data for IL-1 β , caspase-1, NLRP1, and NLRP3 in immunopanned CD31 $^{+}$ endothelial cells, CD11b $^{+}$ myeloid cells, CD13 $^{+}$ pericytes, and negatively selected neurons in sham versus 3HD mice brain at 14 months after injury. Pro IL-1 β in male CD31 $^{+}$ $p = 0.14$, CD11b $^{+}$ $p = 0.93$, CD13 $^{+}$ $p = 0.61$, neurons $p = 0.045$, in female neurons $p = 0.97$, t tests; cleaved IL-1 β in male neurons $p = 0.018$, in female neurons $p = 0.34$ t test; pro caspase 1 in male CD31 $^{+}$ $p = 0.60$, CD11b $^{+}$ $p = 0.36$; CD13 $^{+}$ $p = 0.79$; neurons $p = 0.13$, in female neurons $p = 0.68$, t tests; cleaved caspase 1 in male neurons $p = 0.025$; NLRP3 in male CD31 $^{+}$ $p = 0.54$; CD11b $^{+}$ $p = 0.021$; CD13 $^{+}$ $p = 0.048$, neurons $p = 0.51$, t tests; NLRP1 in male CD31 $^{+}$ $p = 0.79$; CD11b $^{+}$ $p = 0.53$; CD13 $^{+}$ $p = 0.76$; neurons $p = 0.048$, in female neurons $p = 0.54$, t tests ($n = 4$ –6/group).

females (Fig. 5A–E), confirming that the IL-1 β response in 3HD mice correlates with cognitive dysfunction. Notably, IL-1 β and caspase-1 cleavage was not readily detected in CD31 $^{+}$ cells, CD11b $^{+}$ cells, or CD13 $^{+}$ cells at 14 months. At 14 months, expression of full-length NLRP1 was significantly decreased in neurons isolated from 3HD versus sham in males but not in females, consistent with activation (Fig. 5A,F). NLRP3 was increased in CD11b $^{+}$ cells in males, whereas expression of NLRP3 was not detected in neurons both in males and females (Fig. 5A,G).

Tau aggregation after 3HD in adolescent mice

Pathologic IL-1 β activation may occur upstream or downstream of aberrant tau hyperphosphorylation, and both events are associated with cognitive deficits in AD and tauopathy models (Collins-Praino and Corrigan, 2017). To evaluate pathologic tau activation, we examined tau and phospho-tau expression in detergent-soluble (Triton X-100) and insoluble (8 M urea) fractions from immunopanned CD31 $^{+}$, CD11b $^{+}$, CD13 $^{+}$ cells and neurons at 14 months after sham and 3HD. No changes in AT8 reactivity between groups were observed in any of the cell types in the Triton X-100 fractions of male mice, except that injured mice had significantly less AT8 immunoreactivity in CD31 $^{+}$ cells (Extended Data Fig. 6-1A,B). In males, reactivity with the AT8 antibody was significantly increased in urea-soluble fractions of 3HD neurons versus sham, decreased in CD31 $^{+}$ cells, and unchanged in the CD11b $^{+}$ and CD13 $^{+}$ cells (Fig. 6A,B and Extended data Fig. 5-2B). However, AT8 immunoreactivity was not different in female 3HD neurons versus sham in urea-soluble fraction (Fig. 6A,B). No differences were observed between groups in expression of total tau (tau5 antibody) in detergent-soluble or urea-soluble fractions in males or females (Extended Data Fig. 6-1A,C; Fig. 6A,C). Interestingly, AT8 but not tau5 (total tau) immunoreactivity was increased in the urea fraction of neurons from 1HD mice (Extended Data Fig. 6-1D–F). CP13 (pSer 202 tau) immunoreactivity was increased in Triton X-100-soluble fractions but not in the urea fraction, whereas MC1,

specific for phospho-tau tangle conformation (Tau5-15/312-322 tau) and PHF-1 (pSer396/pSer404 tau), each showed increased reactivity in the urea fraction (but not in Triton X-100-soluble fractions) in neurons from male 3HD versus sham (Fig. 6D,E; Extended Data Fig. 6-1G–J). However, females did not show changes in CP13, MC1, and PHF1 in the urea fraction of isolated neurons from 3HD versus sham (Fig. 6D,F). These data suggest that adolescent 3HD induces tau hyperphosphorylation and aggregation in neurons of male mice. However, immunohistochemical analyses did not detect pathologic tau species in brain sections from sham or 3HD mice, indicating that the change in cell compartment of phospho-tau was not detectable by IHC methods (Extended Data Fig. 6-2). The tau kinase phospho-CAMKII, a key enzyme mediating tau hyperphosphorylation in neurodegenerative diseases, was also increased in 3HD neurons from males but not females, suggesting one mechanism of increased phospho-Tau accumulation; however, no changes were observed in another tau kinase GSK3 β in males or females (Fig. 6G–I). Additionally, no differences were observed in TDP43 in 3HD and sham males in the urea fraction of isolated neurons at 14 months (Extended Data Fig. 6-1K,L).

Evidence of impaired proteostasis at the protein level in neurons at 14 months after 3HD

In addition to evidence for inflammasome activation and aberrant Tau accumulation, we observed increased levels of phospho-S6, indicating activation of the mTOR pathway, as well as phospho-Akt, an upstream regulator of mTOR signaling, in male but not female neurons at 14 months after 3HD (Fig. 7A–C). Phospho-EIF2a, which functions to inhibit early steps of protein synthesis, was also increased in male but not female neurons at 14 months (Fig. 7A–C).

Repetitive CHI induces IL-1R1-dependent mechanisms of inflammation

Given evidence of inflammasome activation and increased phospho-Tau in injured neurons, we next sought to investigate IL-

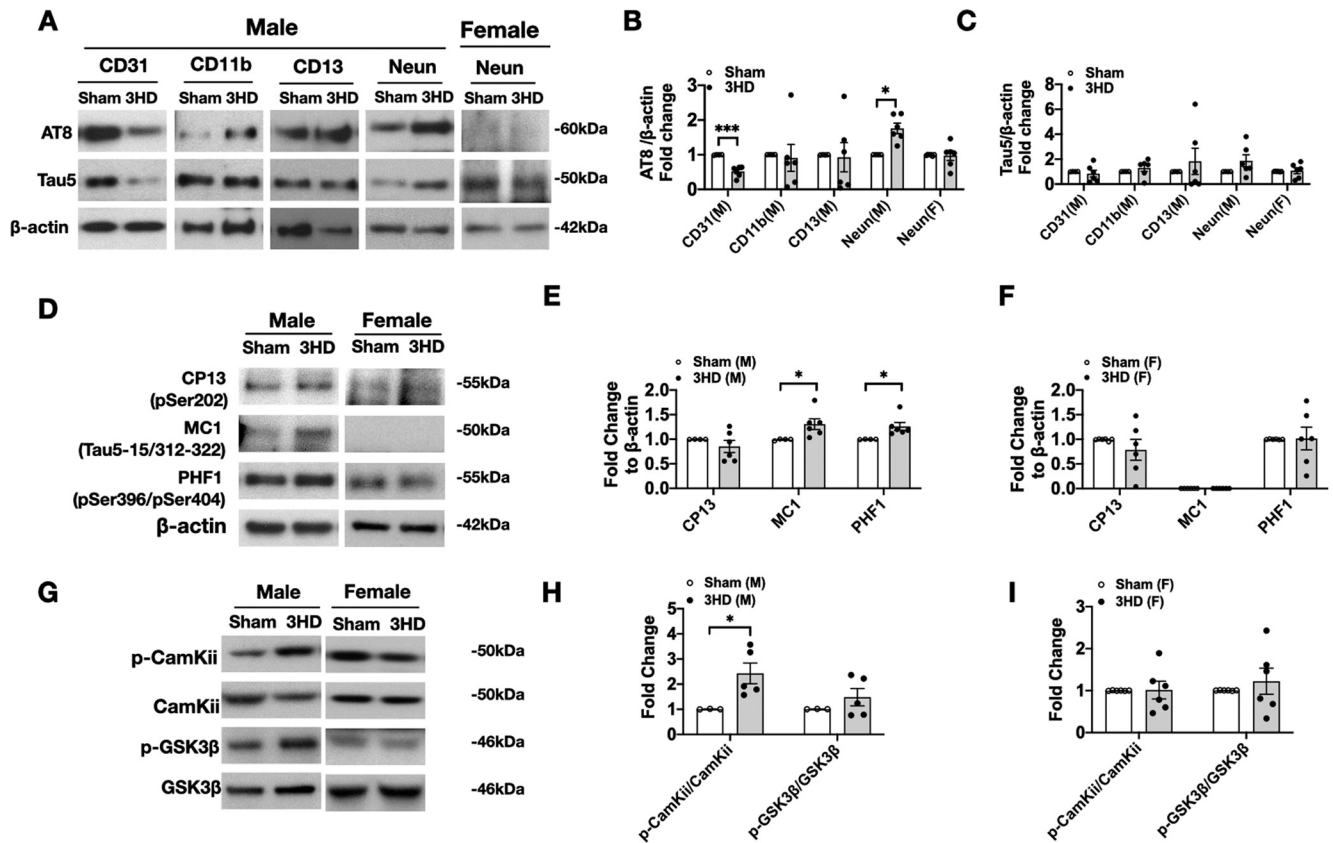


Figure 6. Pathologic tau phosphorylation and aggregation after 3HD. **A**, Representative Western blots and **(B,C)** densitometry analyses for phosphorylated-Tau (AT8) and total-Tau (Tau5) expression in detergent (Triton X-100)-insoluble (8 M urea-soluble) cell fractions from immunopanned CD31⁺, CD11b⁺, CD13⁺ cells and negatively selected neurons at 14 months after sham and 3HD. pTau expression was increased in neurons from 3HD versus sham in males ($p = 0.0039$, t test) but not in females ($p = 0.76$, $n = 6$ /group), decreased in male CD31 versus sham ($p = 0.00026$, t test), and unchanged in male CD11b⁺ ($p = 0.85$) and male CD13⁺ ($p = 0.90$) cells versus sham. No change in total tau (detected by Tau5) was observed in any cell types at 14 months (males: CD31⁺, $p = 0.67$; CD11b⁺, $p = 0.43$; CD13⁺, $p = 0.55$; neurons, $p = 0.19$; $n = 4$ -6/group, females: neurons, $p = 0.78$, $n = 6$ /group, t tests). **D**, Representative Western blots and **(E)** densitometry analyses of pSer202 tau (CP13), conformation-specific tau (tau5-15/312-322, MC1), and pSer396/pSer404 tau (PHF1) in detergent-insoluble fractions of neurons at 14 months showing increased tau5-15/312-322 ($p = 0.047$) and pSer396/pSer404 tau ($p = 0.035$) but not pSer202 tau ($p = 0.38$) versus sham in males ($n = 4$ -6/group, t tests), but no difference in CP13 ($p = 0.35$), MC1 (not detected), or PHF1 ($p = 0.94$) between 3HD versus sham in females (F , $n = 6$ /group, t tests). **G–I**, Representative Western blot (**G**) and densitometry analyses of the tau kinases p-CAMKII and p-GSK-3β in 3HD versus sham in **(H)** males (p-CAMKII: $*p = 0.042$; p-GSK-3β: $p = 0.35$; $n = 3$ -5/group, t tests) and **(I)** females (p-CAMKII: $p = 0.95$; p-GSK-3β: $p = 0.5$; $n = 6$ /group, t tests) at 14 months after injury.

IL1R1-dependent inflammation in 3HD mice. To this end, male and female *IL1R1*^{-/-} mice were subjected to sham or 3HD, and behavioral outcomes were compared at 6 months followed by Western blot analysis of brain tissue homogenates. Body weights were not different between male sham and 3HD *IL1R1*^{-/-} mice (Fig. 8A). In the rotarod test, 3HD male *IL1R1*^{-/-} mice performed significantly worse than sham (Fig. 8B). However, we did not detect differences between groups in a forced swim test (Fig. 8C) or MWM (Fig. 8D–F) in male *IL1R1*^{-/-} mice. In females, percent time spent in the open arms in an elevated plus maze did not differ between sham and 3HD *IL1R1*^{-/-} mice at 3 months after injury (Fig. 8G), whereas WT 3HD female mice showed significantly decreased time on the open arms versus sham (Fig. 2G). In addition, Western blot analyses showed that pro-IL-1β (Fig. 8H–J) was increased in cortex and cerebellum of injured male WT but not *IL1R1*^{-/-} mice, and AT8 (Fig. 8K–M) immunoreactivity was increased in cortex of 3HD male WT but not *IL1R1*^{-/-} mice, suggesting that IL-1R1 regulates tau phosphorylation and IL-1β accumulation in injured brain during the chronic period in male mice.

Discussion

Epidemiological data suggest that repetitive TBI is associated with neurodegenerative disease. In this study, we elucidate

neuronal mechanisms underlying this phenomenon with a focus on the adolescent age group (Tagge et al., 2018). We found that 3HD in adolescent mice (38–40 d old, approximating brain development of an early teenage human) (Flurkey et al., 2007) induced delayed, progressive cognitive deficits associated with impaired proteostasis, the dynamic processes regulating protein synthesis, folding, trafficking, and degradation. We found activation of the mTOR pathway and the inflammasome, as well as upregulation of a Tau kinase and accumulation of hyperphosphorylated, misfolded Tau, 14 months after injury (approximating 47 years in humans) (Flurkey et al., 2007). Hyperphosphorylated tau is associated with neurofibrillary tangles in AD and CTE, and inhibition of tau kinases, such as GSK3β and CDK5, has been a top research strategy to inhibit pathologic tau accumulation and prevent neurodegenerative diseases (Breen and Krishnan, 2020). Notably, *IL1R1*^{-/-} mice did not accumulate phospho-Tau in injured cerebellum. Given our prior report that *IL1R1*^{-/-} mice are protected from acute postinjury cognitive deficits after 3HD (Wu et al., 2019), these results suggest that IL-1R1 activity may drive cognitive deficits and phospho-tau accumulation, as well as generation of the inactive pro-form of IL-1β (31 kDa), in a feedforward loop after 3HD in adolescent mice. Our data provide cell-specific molecular mechanisms by which youth exposure to repetitive mTBI might reduce resiliency to neurologic dysfunction later in life (Alosco et al., 2018).

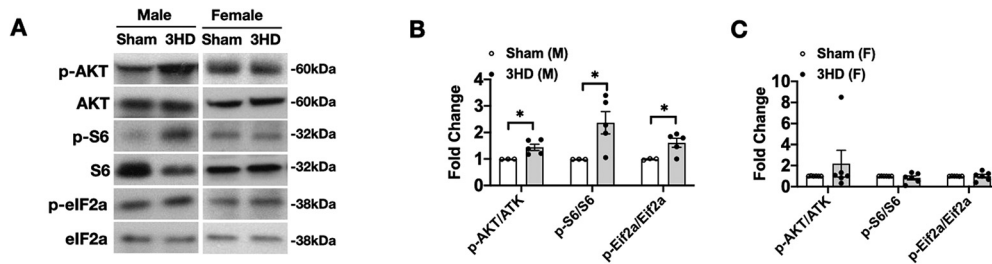


Figure 7. Altered expression of proteins involved in proteostasis in neurons at 14 months after 3HD. **A**, Representative Western blots and (**B**, **C**) densitometry analyses of phosphorylated and total AKT, S6, and eIF2a in male (**B**) and female (**C**) neurons at 14 months. Male: p-AKT/ATK, $*p = 0.030$; p-S6/S6, $*p = 0.049$; p-eIF2a/eIF2a, $*p = 0.036$, $n = 3$ –5/group, t test. Female: p-AKT/ATK, $p = 0.38$; p-S6/S6, $p = 0.4$; p-eIF2a/eIF2a, $p = 0.98$, $n = 6$ /group, t test.

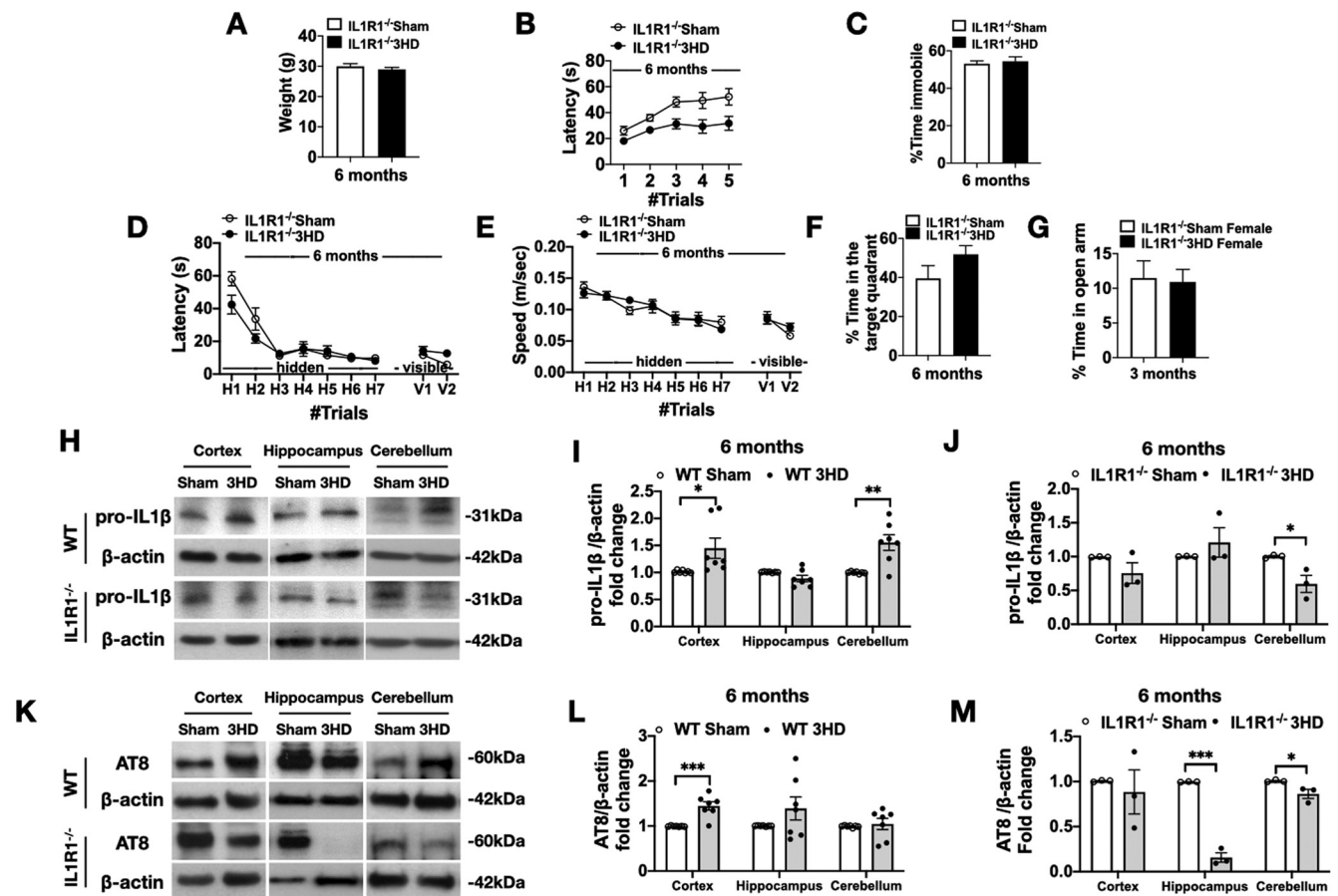


Figure 8. Reduced inflammation and tau aggregation after 3HD in mice deficient in IL-1R1. **A**, Body weight at 6 months after sham and 3HD in male $IL1R1^{-/-}$ mice ($p = 0.39$, $n = 5$ –10/group, t test). **B**, Rotarod test performance was worse in 3HD male $IL1R1^{-/-}$ versus sham at 6 months (two-way repeated-measures ANOVA, $F_{(1,13)} = 6.93$, $p = 0.021$ for group, $n = 5$ –10/group). **C**, Immobility in the forced swim test was similar between sham and 3HD male $IL1R1^{-/-}$ mice at 6 months ($p = 0.74$, $n = 5$ –10/group, t test). **D**, In male $IL1R1^{-/-}$ mice, MWM hidden and visible platform performance was similar in 3HD and sham at 6 months (two-way repeated-measures ANOVA, hidden: $F_{(1,13)} = 3.6$, $p = 0.08$ for group; visible: $F_{(1,13)} = 4.26$, $p = 0.06$ for group; $n = 5$ –10/group). **E**, Swim speed in the MWM did not differ between sham and 3HD male $IL1R1^{-/-}$ mice (two-way repeated-measures ANOVA, hidden: $F_{(1,13)} = 0.01$, $p = 0.92$ for group; visible: $F_{(1,13)} = 0.43$, $p = 0.52$ for group; $n = 5$ –10/group). **F**, Probe trial performance did not differ between male sham and 3HD $IL1R1^{-/-}$ mice at 6 months ($p = 0.14$, $n = 5$ –10/group, t test). **G**, In an elevated plus maze, 3HD female $IL1R1^{-/-}$ mice performed similar to sham at 3 months after injury ($p = 0.86$, $n = 13$ –15/group, t test). **H**, Western blot and (**I**, **J**) densitometry analyses of pro-IL1 β expression in homogenates of cortex, hippocampus, and cerebellum at 6 months after injury in male WT and $IL1R1^{-/-}$ mice ($n = 3$ –7/group). Pro-IL1 β expression was increased in 3HD versus sham in cortex and cerebellum in WT (**I**) but not in $IL1R1^{-/-}$ (**J**) mice (WT cortex, $*p = 0.040$; hippocampus, $p = 0.068$; cerebellum, $**p = 0.0023$; $IL1R1^{-/-}$ cortex, $p = 0.19$; hippocampus, $p = 0.40$; cerebellum, $*p = 0.033$; $n = 3$ –7/group, t test). **K**, Western blot and (**L**, **M**) densitometric analyses of AT8 expression in detergent-insoluble (urea-soluble) homogenates of cortex, hippocampus, and cerebellum showing increased AT8 aggregation in 3HD versus sham in cortex in WT (**L**) but not in $IL1R1^{-/-}$ (**M**) mice at 6 months after injury (WT cortex, $***p = 0.00038$; hippocampus $p = 0.15$; cerebellum, $p = 0.68$; $IL1R1^{-/-}$ cortex, $p = 0.64$; hippocampus, $***p < 0.001$; cerebellum, $*p = 0.047$; $n = 3$ –7/group, t test).

However, since we did not study an adult comparison group, we cannot rule out the possibility that these changes may occur independent of the age at injury.

We found marked differences in the neurologic and biochemical responses to 3HD in female versus male mice, with female

mice protected from cognitive deficits but uniquely vulnerable to postinjury anxiety as suggested by reduced time in the open arms in the elevated plus maze. Female mice also lacked the protein biochemical abnormalities observed in neurons of 3HD male mice at 14 months. One possible explanation for these data

is that the biomechanics of CHI produce less severe injury in female mice, which weigh significantly less than males. This possibility is tempered by the finding that righting reflex times were not different between 3HD males and females and that, like injured males, injured females had rotarod deficits. Nonetheless, further studies (with increasing injury severity levels) are needed to determine whether females are truly resistant to cognitive dysfunction and abnormal proteostasis observed in 3HD males.

Impaired neuronal proteostasis and spatial learning deficits in males occurred in the absence of histologically detectable tau tangles or β amyloid plaques. It is possible that 3HD induces a biochemical phase of injury lasting decades in humans until cellular homeostatic mechanisms fail, leading to cellular and clinical phases of neurodegenerative disease. In this scenario, dysregulation of neural gene networks that occur during early stages of repetitive mTBI may be exacerbated by aging, genetic, or environmental factors, leading to an irreversible stage of neurodegeneration in vulnerable individuals. This theoretical framework has been hypothesized to underlie vulnerability to sporadic AD (De Strooper and Karran, 2016; Van Eldik et al., 2016; Meyer et al., 2019).

Despite a considerable literature associating TBI with prolonged neuroinflammation and increased risk for AD, CTE, and dementia (Faden and Loane, 2015), the exact mechanisms by which early life TBI leads to later cognitive dysfunction remain undefined. A growing number of studies suggest an important contribution of inflammasome signaling to functional outcome in acute TBI (de Rivero Vaccari et al., 2009, 2016; Adamczak et al., 2012, 2014; Kerr et al., 2018) and neurodegenerative diseases (Voet et al., 2019). We detected evidence of inflammasome activation (cleavage of NLRP1, caspase-1, and IL-1 β to active fragments) in neurons at 14 months after 3HD, as well as increased pro-IL-1 β in brain tissue at 6 months. To our knowledge, our data are the first to demonstrate neuronal inflammasome activation at >1 year in a repetitive mTBI rodent model. IL-1 β impairs synaptic transmission (O'Connor and Coogan, 1999), and genetic deletion of IL-1R1 or caspase-1/11 reduced cognitive deficits after single and repetitive CHI in adult and adolescent mice, respectively, suggesting that inflammasome activity contributes to cognitive dysfunction in CHI models (Chung et al., 2019; Wu et al., 2019).

In mouse familial AD models, NLRP3 inflammasome activation in microglia plays a key role in impairment of LTP and cognitive dysfunction (Heneka et al., 2013; Dempsey et al., 2017; Flores et al., 2018). Similarly, antagonism of the NLRP3 inflammasome alleviated the detrimental effects of systemic immune stimulation on LTP and cognitive function in the aging brain (Dempsey et al., 2017; Flores et al., 2018; Beyer et al., 2020). The neuronal NLRP1 inflammasome has also been hypothesized to contribute to AD, as NLRP1 immunoreactivity was upregulated in brains of AD patients (Yap et al., 2019), and cultured human neurons activate a NLRP1/caspase-1 inflammasome in AD (Kaushal et al., 2015). Genetic variants of NLRP1 are associated with AD risk (Pontillo et al., 2012), and NLRP1 knock-down rescues cognitive deficits in AD transgenic mice (Tan et al., 2014). Prolonged overexpression of IL-1 β does not necessarily lead to neuronal cell death, even in Tau transgenic mice (Shaftel et al., 2007; Matousek et al., 2012), and the effects of IL-1 β activation at 14 months after 3HD do not appear overwhelming and may be reversible by pharmacological inhibitors. Our results imply that targeting NLRP1 inflammasomes might be needed to ameliorate cognitive deficits after repetitive mTBI.

In animal studies, direct links between repetitive mTBI and CTE have remained elusive, in part because no repetitive mTBI model has recapitulated the unique pathognomonic neuropathological features of CTE, including accumulation of phospho-tau in neurons and astrocytes in a perivascular distribution (McKee, 2020). Some groups have reported increased phosphorylated Tau in the chronic period after repetitive mTBI, whereas others have not (Bachstetter et al., 2020), even in mice expressing human tau isoforms (Gangolli et al., 2019; Mouzon et al., 2019). In contrast, repetitive mTBI accelerated the onset of tau hyperphosphorylation in the optic tracts of adolescent mice carrying human tau transgenes predisposed to tau aggregation (Xu et al., 2015). We detected hyperphosphorylated, misfolded tau in neurons at 1 year after 3HD; however, we did not detect pathologic tau or β amyloid in brain tissue sections of 3HD mice. Rather than recapitulating CTE, our data suggest that repetitive mTBI in adolescents may initiate changes in neuronal proteostasis and inflammation that could lead to increased risk later in life of a variety of neurodegenerative diseases which feature protein aggregates (McAlary et al., 2020; Sonninen et al., 2020).

We found that adolescent mice lacking IL-1R1 had no increase in phosphorylated Tau in cerebellar brain homogenates at 6 months after 3HD. These data suggest a regulatory role for IL-1R1 in the pathogenesis of phospho-tau accumulation after repetitive head injury. IL-1 β activates kinases that promote tau hyperphosphorylation (Collins-Praino and Corrigan, 2017), such as CAMKII- α , which was increased in neurons at 14 months in the current study. Exposure of mouse brain or neuron-microglia cocultures to IL-1 β increases tau phosphorylation at multiple sites (Sheng et al., 2000; Li et al., 2003) attributable in part to increased activity of tau kinases (Cho and Johnson, 2003; Ghosh et al., 2013), and chronic administration of IL-1R or genetic deletion of NLRP3 or ASC inhibits tau phosphorylation (Kitazawa et al., 2011) in part by reducing CAMKII α activation and enhancing tau phosphatase activity (Heneka et al., 2013; Ising et al., 2019). Neurons cocultured with activated, pro-inflammatory microglia had increased CAMKII- α and pTau, which was dependent on neuronal IL-1R1 (Ising et al., 2019). Our finding that IL-1R1 $^{-/-}$ prevented increased phospho-Tau levels in cortex and cerebellum suggests that inflammasome activation drives Tau phosphorylation in repetitive CHI. On the other hand, expression of human mutant Tau in mice caused brain inflammation and inhibited the ER stress response (Hull et al., 2020), suggesting that aberrantly phosphorylated Tau may also contribute to neuronal IL-1 β production and impaired proteostasis in feedforward loops. Impaired proteostasis itself may also lead to accumulation of phosphorylated tau, as pharmacological enhancement of autophagy flux decreases tau $^{+}$ neurons and neuronal death in P301S human mutant tau transgenic mice (Schaeffer et al., 2012). Impaired autophagy increases proinflammatory microglia that contribute to neuronal death in neurodegenerative diseases (Plaza-Zabala et al., 2017), and autophagic elimination of damaged mitochondria attenuates NLRP3 inflammasome activation in macrophages (Zhong et al., 2018). Whether a similar mechanism attenuates NLRP1 inflammasomes in neurons is unknown. Further studies are needed to uncover initiating and propagating mechanisms of inflammasome activation, as well as the relationship between IL-1R1 and impaired proteostasis in repetitive mTBI models.

Future directions

Key differences exist between human and mouse inflammasomes. Humans have only a single NLRP1 gene, while mice have

three NLRP1 isoforms. Similarly, humans have two orthologs for caspase-11, viz. caspase-4 and caspase-5 (Lamkanfi and Dixit, 2012). More research using human cell types, eventually based on iPSC technology and patient-derived material, will be needed to translate findings more effectively from rodents to the human conditions they model. We found that females had several interesting phenotypes after 3HD, including motor learning and anxiety, but not cognitive function phenotypes versus sham. Because females did not show cognitive deficits at 1 year after 3HD, we only studied proteostasis pathways in males, but it is likely that the cellular and molecular consequences of repetitive mTBI differ in male and female brains, and future studies will be needed to assess this important question. As with any RNA Seq dataset, examining more cells would be helpful to more fully interpret transcriptomic changes in glial and other cell types. Addressing this question will require further studies enriching for microglia and astrocytes.

References

- Adamczak S, Dale G, de Rivero Vaccari JP, Bullock MR, Dietrich WD, Keane RW (2012) Inflammasome proteins in cerebrospinal fluid of brain-injured patients as biomarkers of functional outcome: clinical article. *J Neurosurg* 117:1119–1125.
- Adamczak S, de Rivero Vaccari JP, Dale G, Brand FJ, Nonner D, Bullock MR, Dahl GP, Dietrich WD, Keane RW (2014) Pyroptotic neuronal cell death mediated by the AIM2 inflammasome. *J Cereb Blood Flow Metab* 34:621–629.
- Alonso ML, Mez J, Tripodis Y, Kiernan PT, Abdolmohammadi B, Murphy L, Kowall NW, Stein TD, Huber BR, Goldstein LE, Cantu RC, Katz DI, Chaisson CE, Martin B, Solomon TM, McClean MD, Daneshvar DH, Nowinski CJ, Stern RA, McKee AC (2018) Age of first exposure to tackle football and chronic traumatic encephalopathy. *Ann Neurol* 83:886–901.
- Apelt J, Kumar A, Schliebs R (2002) Impairment of cholinergic neurotransmission in adult and aged transgenic Tg2576 mouse brain expressing the Swedish mutation of human beta-amyloid precursor protein. *Brain Res* 953:17–30.
- Bachstetter AD, Morganti JM, Bodnar CN, Webster SJ, Higgins EK, Roberts KN, Snider H, Meier SE, Nation GK, Goulding DS, Hamm M, Powell DK, Vandsburger M, Van Eldik LJ, Abisambra JF (2020) The effects of mild closed head injuries on tauopathy and cognitive deficits in rodents: primary results in wild type and rTg4510 mice, and a systematic review. *Exp Neurol* 326:113180.
- Baillargeon A, Lassonde M, Leclerc S, Ellemberg D (2012) Neuropsychological and neurophysiological assessment of sport concussion in children, adolescents and adults. *Brain Inj* 26:211–220.
- Barlow KM (2016) Postconcussion syndrome: a review. *J Child Neurol* 31:57–67.
- Barlow KM, Crawford S, Stevenson A, Sandhu SS, Belanger F, Dewey D (2010) Epidemiology of postconcussion syndrome in pediatric mild traumatic brain injury. *Pediatrics* 126:e374–81.
- Beyer MM, Lonnemann N, Remus A, Latz E, Heneka MT, Korte M (2020) Enduring changes in neuronal function upon systemic inflammation are NLRP3 inflammasome dependent. *J Neurosci* 40:5480–5494.
- Binney ZO, Bachynski KE (2019) Estimating the prevalence at death of CTE neuropathology among professional football players. *Neurology* 92:43–45.
- Breen PW, Krishnan V (2020) Recent preclinical insights into the treatment of chronic traumatic encephalopathy. *Front Neurosci* 14:616.
- Cagnetta R, Wong HH, Frese CK, Mallucci GR, Krijgsveld J, Holt CE (2019) Noncanonical modulation of the eIF2 pathway controls an increase in local translation during neural wiring. *Mol Cell* 73:474–489.e5.
- Casper ST, Golden J, Oreskes N, Largent M, Goldberg DS, Gillett G, Philpott-Jones S, Moreira T, Virdi J, Meyers T, Morrison D, Rodriguez JE, Gabriel JM, Steere-Williams J, Ross R, Smith JM, Ballenger JF, Bil G, Kawaguchi Y, Dyck E, et al. (2019) First report the findings: genuine balance when reporting CTE. *Lancet Neurol* 18:522–523.
- Centers for Disease Control and Prevention (2011) Nonfatal traumatic brain injuries related to sports and recreation activities among persons aged < 19 years: United States, 2001–2009. *MMWR Morb Mortal Wkly Rep* 60:1337–1342.
- Centers for Disease Control and Prevention (2017) Traumatic brain injury-related emergency department visits, hospitalizations, and deaths: United States, 2007 and 2013. *MMWR Surveill Summ* 66:1–16.
- Cho JH, Johnson GV (2003) Glycogen synthase kinase 3beta phosphorylates tau at both primed and unprimed sites: differential impact on microtubule binding. *J Biol Chem* 278:187–193.
- Choe MC, Babikian T, DiFiori J, Hovda DA, Giza CC (2012) A pediatric perspective on concussion pathophysiology. *Curr Opin Pediatr* 24:689–695.
- Chung JY, Krapp N, Wu L, Lule S, McAllister LM, Edmiston WJ, Martin S, Levy E, Songtchalert T, Sherwood JS, Buckley EM, Sanders B, Izzy S, Hickman S, Guo S, Lok J, El Khoury J, Lo EH, Kaplan D, Whalen MJ 3rd (2019) Interleukin-1 receptor 1 deletion in focal and diffuse experimental traumatic brain injury in mice. *J Neurotrauma* 36:370–379.
- Colacurcio DJ, Nixon RA (2016) Disorders of lysosomal acidification: the emerging role of v-ATPase in aging and neurodegenerative disease. *Ageing Res Rev* 32:75–88.
- Collins-Praino LE, Corrigan F (2017) Does neuroinflammation drive the relationship between tau hyperphosphorylation and dementia development following traumatic brain injury? *Brain Behav Immun* 60:369–382.
- de Rivero Vaccari JP, Lotocki G, Alonso OF, Bramlett HM, Dietrich WD, Keane RW (2009) Therapeutic neutralization of the NLRP1 inflammasome reduces the innate immune response and improves histopathology after traumatic brain injury. *J Cereb Blood Flow Metab* 29:1251–1261.
- de Rivero Vaccari JP, Dietrich WD, Keane RW (2016) Therapeutics targeting the inflammasome after central nervous system injury. *Transl Res* 167:35–45.
- De Strooper B, Karran E (2016) The cellular phase of Alzheimer's disease. *Cell* 164:603–615.
- Dempsey C, Rubio Araiz A, Bryson KJ, Finucane O, Larkin C, Mills EL, Robertson AA, Cooper MA, O'Neill LA, Lynch MA (2017) Inhibiting the NLRP3 inflammasome with MCC950 promotes non-phlogistic clearance of amyloid-beta and cognitive function in APP/PS1 mice. *Brain Behav Immun* 61:306–316.
- Deshpande SK, Hasegawa RB, Rabinowitz AR, Whyte J, Roan CL, Tabatabaei A, Baiocchi M, Karlawish JH, Master CL, Small DS (2017) Association of playing high school football with cognition and mental health later in life. *JAMA Neurol* 74:909–918.
- Faden AI, Loane DJ (2015) Chronic neurodegeneration after traumatic brain injury: Alzheimer disease, chronic traumatic encephalopathy, or persistent neuroinflammation? *Neurotherapeutics* 12:143–150.
- Farris W, Schütz SG, Cirrito JR, Shankar GM, Sun X, George A, Leissring MA, Walsh DM, Qiu WQ, Holtzman DM, Selkoe DJ (2007) Loss of neprilysin function promotes amyloid plaque formation and causes cerebral amyloid angiopathy. *Am J Pathol* 171:241–251.
- Faul M, Xu L, Wald M, Coronado VG (2010) Traumatic brain injury in the United States: emergency department visits, hospitalizations and deaths, 2002–2006. Atlanta: Centers for Disease Control and Prevention.
- Field M, Collins MW, Lovell MR, Maroon J (2003) Does age play a role in recovery from sports-related concussion? A comparison of high school and collegiate athletes. *J Pediatr* 142:546–553.
- Flores J, Noel A, Foveau B, Lynham J, Lecrux C, LeBlanc AC (2018) Caspase-1 inhibition alleviates cognitive impairment and neuropathology in an Alzheimer's disease mouse model. *Nat Commun* 9:3916.
- Flurkey KJ, Currer DE, Harrison (2007) The mouse in aging research. Burlington, MA: Elsevier.
- Gangolli M, Benetos J, Esparza TJ, Fountain EM, Seneviratne S, Brody DL (2019) Repetitive concussive and subconcussive injury in a human tau mouse model results in chronic cognitive dysfunction and disruption of white matter tracts, but not tau pathology. *J Neurotrauma* 36:735–755.
- Gardner RC, Yaffe K (2015) Epidemiology of mild traumatic brain injury and neurodegenerative disease. *Mol Cell Neurosci* 66:75–80.
- Geyer M, Fackler OT, Peterlin BM (2002) Subunit H of the V-ATPase involved in endocytosis shows homology to beta-adaptins. *Mol Biol Cell* 13:2045–2056.
- Ghosh S, Wu MD, Shaftel SS, Kyrkanides S, LaFerla FM, Olschowka JA, O'Banion MK (2013) Sustained interleukin-1beta overexpression exacerbates tau pathology despite reduced amyloid burden in an Alzheimer's mouse model. *J Neurosci* 33:5053–5064.
- Gingras S, Earls LR, Howell S, Smeyne RJ, Zakharenko SS, Pelletier S (2015) SCYL2 protects CA3 pyramidal neurons from excitotoxicity during

- functional maturation of the mouse hippocampus. *J Neurosci* 35:10510–10522.
- Giovedì S, Ravanelli MM, Parisi B, Bettgazzi B, Guarnieri FC (2020) Dysfunctional autophagy and endolysosomal system in neurodegenerative diseases: relevance and therapeutic options. *Front Cell Neurosci* 14:602116.
- Giza CC, Prins ML (2006) Is being plastic fantastic? Mechanisms of altered plasticity after developmental traumatic brain injury. *Dev Neurosci* 28:364–379.
- Grant DA, Serpa R, Moattari CR, Brown A, Greco T, Prins ML, Teng E (2018) Repeat mild traumatic brain injury in adolescent rats increases subsequent beta-amyloid pathogenesis. *J Neurotrauma* 35:94–104.
- Halstead ME, Walter KD, Council on Sports Medicine and Fitness (2010) American Academy of Pediatrics. Clinical report—sport-related concussion in children and adolescents. *Pediatrics* 126:597–615.
- Harmon KG, Drezner J, Gammons M, Guskiewicz K, Halstead M, Herring S, Kutcher J, Pana A, Putukian M, Roberts W, American Medical Society for Sports Medicine (2013) American Medical Society for Sports Medicine position statement: concussion in sport. *Clin J Sport Med* 23:1–18.
- Heneka MT, Kummer MP, Stutz A, Delekate A, Schwartz S, Vieira-Saecker A, Griep A, Axt D, Remus A, Tzeng TC, Gelpi E, Halle A, Korte M, Latz E, Golenbock DT (2013) NLRP3 is activated in Alzheimer's disease and contributes to pathology in APP/PS1 mice. *Nature* 493:674–678.
- Hessen E, Nestvold K, Anderson V (2007) Neuropsychological function 23 years after mild traumatic brain injury: a comparison of outcome after paediatric and adult head injuries. *Brain Inj* 21:963–979.
- Hoyaux D, Boom A, Van den Bosch L, Belot N, Martin JJ, Heizmann CW, Kiss R, Pochet R (2002) S100A6 overexpression within astrocytes associated with impaired axons from both ALS mouse model and human patients. *J Neuropathol Exp Neurol* 61:736–744.
- Hull C, Dekeryte R, Koss DJ, Crouch B, Buchanan H, Delibegovic M, Platt B (2020) Knock-in of mutated hTAU causes insulin resistance, inflammation and proteostasis disturbance in a mouse model of frontotemporal dementia. *Mol Neurobiol* 57:539–550.
- Ising C, Venegas C, Zhang S, Scheiblich H, Schmidt SV, Vieira-Saecker A, Schwartz S, Albasset S, McManus RM, Tejera D, Griep A, Santarelli F, Brosseron F, Opitz S, Stunden J, Merten M, Kaye R, Golenbock DT, Blum D, Latz E, et al. (2019) NLRP3 inflammasome activation drives tau pathology. *Nature* 575:669–673.
- Jin S, Guerrero-Juarez CF, Zhang L, Chang I, Ramos R, Kuan CH, Myung P, Plikus MV, Nie Q (2021) Inference and analysis of cell-cell communication using CellChat. *Nat Commun* 12:1088.
- Kalish BT, Kim E, Finander B, Duffy EE, Kim H, Gilman CK, Yim YS, Tong L, Kaufman RJ, Griffith EC, Choi GB, Greenberg ME, Huh JR (2021) Maternal immune activation in mice disrupts proteostasis in the fetal brain. *Nat Neurosci* 24:204–213.
- Kaushal V, Dye R, Pakavathkumar P, Foveau B, Flores J, Hyman B, Ghetti B, Koller BH, LeBlanc AC (2015) Neuronal NLRP1 inflammasome activation of Caspase-1 coordinately regulates inflammatory interleukin-1-beta production and axonal degeneration-associated Caspase-6 activation. *Cell Death Differ* 22:1676–1686.
- Kerr N, Lee SW, Perez-Barcena J, Crespi C, Ibañez J, Bullock MR, Dietrich WD, Keane RW, de Rivero Vaccari JP (2018) Inflammasome proteins as biomarkers of traumatic brain injury. *PLoS One* 13:e0210128.
- Khuman J, Meehan WP, Zhu X, Qiu J, Hoffmann U, Zhang J, Giovannone E, Lo EH, Whalen MJ (2011) Tumor necrosis factor alpha and Fas receptor contribute to cognitive deficits independent of cell death after concussive traumatic brain injury in mice. *J Cereb Blood Flow Metab* 31:778–789.
- Kitazawa M, Cheng D, Tsukamoto MR, Koike MA, Wes PD, Vasilevko V, Cribbs DH, LaFerla FM (2011) Blocking IL-1 signaling rescues cognition, attenuates tau pathology, and restores neuronal beta-catenin pathway function in an Alzheimer's disease model. *J Immunol* 187:6539–6549.
- Klein AM, Mazutis L, Akartuna I, Tallapragada N, Veres A, Li V, Peshkin L, Weitz DA, Kirschner MW (2015) Droplet barcoding for single-cell transcriptomics applied to embryonic stem cells. *Cell* 161:1187–1201.
- Kriz PK, Mannix R, Taylor AM, Ruggieri D, Meehan WP (2017) Neurocognitive deficits of concussed adolescent athletes at self-reported symptom resolution in the Zurich guidelines era. *Orthop J Sports Med* 5:2325967117737307.
- Lamkanfi M, Dixit VM (2012) Inflammasomes and their roles in health and disease. *Annu Rev Cell Dev Biol* 28:137–161.
- Langlois JA, Rutland-Brown W, Wald MM (2006) The epidemiology and impact of traumatic brain injury: a brief overview. *J Head Trauma Rehabil* 21:375–378.
- Levin H, Hanten G, Max J, Li X, Swank P, Ewing-Cobbs L, Dennis M, Menefee DS, Schachar R (2007) Symptoms of attention-deficit/hyperactivity disorder following traumatic brain injury in children. *J Dev Behav Pediatr* 28:108–118.
- Li Y, Liu L, Barger SW, Griffin WS (2003) Interleukin-1 mediates pathological effects of microglia on tau phosphorylation and on synaptophysin synthesis in cortical neurons through a p38-MAPK pathway. *J Neurosci* 23:1605–1611.
- Liu MY, Yin CY, Zhu LJ, Zhu XH, Xu C, Luo CX, Chen H, Zhu DY, Zhou QG (2018) Sucrose preference test for measurement of stress-induced anhedonia in mice. *Nat Protoc* 13:1686–1698.
- Maetzler W, Stoycheva V, Schmid B, Schulte C, Hauser AK, Brockmann K, Melms A, Gasser T, Berg D (2010) Neprilysin activity in cerebrospinal fluid is associated with dementia and amyloid-beta42 levels in Lewy body disease. *J Alzheimers Dis* 22:933–938.
- Mannix R, Meehan WP, Mandeville J, Grant PE, Gray T, Berglass J, Zhang J, Bryant J, Rezaie S, Chung JY, Peters NV, Lee C, Tien LW, Kaplan DL, Feany M, Whalen M (2013) Clinical correlates in an experimental model of repetitive mild brain injury. *Ann Neurol* 74:65–75.
- Marin JR, Weaver MD, Yealy DM, Mannix RC (2014) Trends in visits for traumatic brain injury to emergency departments in the United States. *JAMA* 311:1917–1919.
- Matousek SB, Ghosh S, Shaftel SS, Kyrkanides S, Olschowka JA, O'Banion MK (2012) Chronic IL-1beta-mediated neuroinflammation mitigates amyloid pathology in a mouse model of Alzheimer's disease without inducing overt neurodegeneration. *J Neuroimmune Pharmacol* 7:156–164.
- McAlary L, Chew YL, Lum JS, Geraghty NJ, Yerbury JJ, Cashman NR (2020) Amyotrophic lateral sclerosis: proteins, proteostasis, prions, and promises. *Front Cell Neurosci* 14:581907.
- McCrorry P, Meeuwisse W, Aubry M, Cantu B, Dvorak J, Echemendia RJ, Engebretsen L, Johnston K, Kutcher JS, Raftery M, Sills A, Benson BW, Davis GA, Ellenbogen RG, Guskiewicz KM, Herring SA, Iverson G, Jordan BD, Kissick J, McCrear M, et al. (2013) Consensus statement on concussion in sport: the 4th International Conference on Concussion in Sport held in Zurich, November 2012. *Clin J Sport Med* 23:89–117.
- McKee AC (2020) The neuropathology of chronic traumatic encephalopathy: the status of the literature. *Semin Neurol* 40:359–369.
- McKee AC, Stern RA, Nowinski CJ, Stein TD, Alvarez VE, Daneshvar DH, Lee HS, Wojtowicz SM, Hall G, Baugh CM, Riley DO, Kubilus CA, Cormier KA, Jacobs MA, Martin BR, Abraham CR, Ikezu T, Reichard RR, Wolozin BL, Budson AE, et al. (2013) The spectrum of disease in chronic traumatic encephalopathy. *Brain* 136:43–64.
- Mecollari V, Nieuwenhuis B, Verhaagen J (2014) A perspective on the role of class III semaphorin signaling in central nervous system trauma. *Front Cell Neurosci* 8:328.
- Meyer K, Feldman HM, Lu T, Drake D, Lim ET, Ling KH, Bishop NA, Pan Y, Seo J, Lin YT, Su SC, Church GM, Tsai LH, Yankner BA (2019) REST and neural gene network dysregulation in iPSC models of Alzheimer's disease. *Cell Rep* 26:1112–1127 e9.
- Mez J, Daneshvar DH, Kiernan PT, Abdolmohammadi B, Alvarez VE, Huber BR, Alosco ML, Solomon TM, Nowinski CJ, McHale L, Cormier KA, Kubilus CA, Martin BM, Murphy L, Baugh CM, Montenegro PH, Chaisson CE, Tripodis Y, Kowall NW, Weuve J, et al. (2017) Clinicopathological evaluation of chronic traumatic encephalopathy in players of American football. *JAMA* 318:360–370.
- Mohajeri MH, Kuehnle K, Li H, Poirier R, Tracy J, Nitsch RM (2004) Anti-amyloid activity of neprilysin in plaque-bearing mouse models of Alzheimer's disease. *FEBS Lett* 562:16–21.
- Mori T, Koyama N, Arendash GW, Horikoshi-Sakuraba Y, Tan J, Town T (2010) Overexpression of human S100B exacerbates cerebral amyloidosis and gliosis in the Tg2576 mouse model of Alzheimer's disease. *Glia* 58:300–314.
- Mouzon B, Bachmeier C, Ojo J, Acker C, Ferguson S, Crynen G, Davies P, Mullan M, Stewart W, Crawford F (2019) Chronic white matter degeneration, but no tau pathology at one-year post-repetitive mild traumatic brain injury in a tau transgenic model. *J Neurotrauma* 36:576–588.
- Nelson R (2006) Potassium channels have a key role in neurodegeneration. *Lancet Neurol* 5:298–299.

- O'Connor JJ, Coogan AN (1999) Actions of the pro-inflammatory cytokine IL-1 beta on central synaptic transmission. *Exp Physiol* 84:601–614.
- Plaza-Zabala A, Sierra-Torre V, Sierra A (2017) Autophagy and microglia: novel partners in neurodegeneration and aging. *Int J Mol Sci* 18:598.
- Pontillo A, Catamo E, Arosio B, Mari D, Crovella S (2012) NALP1/NLRP1 genetic variants are associated with Alzheimer disease. *Alzheimer Dis Assoc Disord* 26:277–281.
- Rabinowitz AR, Li X, McCauley SR, Wilde EA, Barnes A, Hanten G, Mendez D, McCarthy JJ, Levin HS (2015) Prevalence and predictors of poor recovery from mild traumatic brain injury. *J Neurotrauma* 32:1488–1496.
- Schaeffer V, Lavenir I, Ozcelik S, Tolnay M, Winkler DT, Goedert M (2012) Stimulation of autophagy reduces neurodegeneration in a mouse model of human tauopathy. *Brain* 135:2169–2177.
- Schultz V, Stern RA, Tripodis Y, Stamm J, Wrobel P, Lepage C, Weir I, Guenette JP, Chua A, Alosco ML, Baugh CM, Fritts NG, Martin BM, Chaisson CE, Coleman MJ, Lin AP, Pasternak O, Shenton ME, Koerte IK (2018) Age at first exposure to repetitive head impacts is associated with smaller thalamic volumes in former professional American football players. *J Neurotrauma* 35:278–285.
- Shaftel SS, Kyrkanides S, Olschowka JA, Miller JN, Johnson RE, O'Banion MK (2007) Sustained hippocampal IL-1 beta overexpression mediates chronic neuroinflammation and ameliorates Alzheimer plaque pathology. *J Clin Invest* 117:1595–1604.
- Sheng JG, Zhu SG, Jones RA, Griffin WS, Mrak RE (2000) Interleukin-1 promotes expression and phosphorylation of neurofilament and tau proteins in vivo. *Exp Neurol* 163:388–391.
- Smith DH, Johnson VE, Stewart W (2013) Chronic neuropathologies of single and repetitive TBI: substrates of dementia? *Nat Rev Neurol* 9:211–221.
- Solomon GS, Kuhn AW, Zuckerman SL, Casson IR, Viano DC, Lovell MR, Sills AK (2016) Participation in pre-high school football and neurological, neuro-radiological, and neuropsychological findings in later life: a study of 45 retired National Football League players. *Am J Sports Med* 44:1106–1115.
- Sonninen TM, Goldsteins G, Laham-Karam N, Koistinaho J, Lehtonen S (2020) Proteostasis disturbances and inflammation in neurodegenerative diseases. *Cells* 9:2183.
- Stamm JM, Bourlas AP, Baugh CM, Fritts NG, Daneshvar DH, Martin BM, McClean MD, Tripodis Y, Stern RA (2015a) Age of first exposure to football and later-life cognitive impairment in former NFL players. *Neurology* 84:1114–1120.
- Stamm JM, Koerte IK, Muehlmann M, Pasternak O, Bourlas AP, Baugh CM, Giwerc MY, Zhu A, Coleman MJ, Bouix S, Fritts NG, Martin BM, Chaisson C, McClean MD, Lin AP, Cantu RC, Tripodis Y, Stern RA, Shenton ME (2015b) Age at first exposure to football is associated with altered corpus callosum white matter microstructure in former professional football players. *J Neurotrauma* 32:1768–1776.
- Stewart W, Allinson K, Al-Sarraj S, Bachmeier C, Barlow K, Belli A, Burns MP, Carson A, Crawford F, Dams-O'Connor K, Diaz-Arrastia R, Dixon CE, Edlow BL, Ferguson S, Fischl B, Folkert RD, Gentleman S, Giza CC, Grady MS, Helmy A, et al. (2019) Primum non nocere: a call for balance when reporting on CTE. *Lancet Neurol* 18:231–233.
- Tagge CA, Fisher AM, Minaeva OV, Gaudreau-Balderrama A, Moncaster JA, Zhang XL, Wojnarowicz MW, Casey N, Lu H, Kokiko-Cochran ON, Saman S, Ericsson M, Onos KD, Veksler R, Senatorov VV, Kondo A, Zhou XZ, Miry O, Vose LR, Gopaul KR, et al. (2018) Concussion, microvascular injury, and early tauopathy in young athletes after impact head injury and an impact concussion mouse model. *Brain* 141:422–458.
- Tan MS, Tan L, Jiang T, Zhu XC, Wang HF, Jia CD, Yu JT (2014) Amyloid-beta induces NLRP1-dependent neuronal pyroptosis in models of Alzheimer's disease. *Cell Death Dis* 5:e1382.
- Taylor CA, Bell JM, Breiding MJ, Xu L (2017) Traumatic brain injury-related emergency department visits, hospitalizations, and deaths—United States, 2007 and 2013. *MMWR Surveill Summ* 66:1–16.
- Ting JT, Kelley BG, Lambert TJ, Cook DG, Sullivan JM (2007) Amyloid precursor protein overexpression depresses excitatory transmission through both presynaptic and postsynaptic mechanisms. *Proc Natl Acad Sci USA* 104:353–358.
- Van Eldik LJ, Carrillo MC, Cole PE, Feuerbach D, Greenberg BD, Hendrix JA, Kennedy M, Kozauer N, Margolin RA, Molinuevo JL, Mueller R, Ransohoff RM, Wilcock DM, Bain L, Bales K (2016) The roles of inflammation and immune mechanisms in Alzheimer's disease. *Alzheimers Dement (N Y)* 2:99–109.
- Voet S, Srinivasan S, Lamkanfi M, Loo G (2019) Inflammasomes in neuroinflammatory and neurodegenerative diseases. *EMBO Mol Med* 11:e10248.
- Whitehouse PJ, Price DL, Struble RG, Clark AW, Coyle JT, Delon MR (1982) Alzheimer's disease and senile dementia: loss of neurons in the basal forebrain. *Science* 215:1237–1239.
- Wu L, Chung JY, Saith S, Tozzi L, Buckley EM, Sanders B, Franceschini MA, Lule S, Izzy S, Lok J, Edmiston WJ, McAllister LM, Mebane S, Jin G, Lu J, Sherwood JS, Willwerth S, Hickman S, Khoury JE, Lo EH, et al. (2019) Repetitive head injury in adolescent mice: a role for vascular inflammation. *J Cereb Blood Flow Metab* 39:2196–2209.
- Ximerakis M, Lipnick SL, Innes BT, Simmons SK, Adiconis X, Dionne D, Mayweather BA, Nguyen L, Nizioletk Z, Ozek C, Butty VL, Isserlin R, Buchanan SM, Levine SS, Regev A, Bader GD, Levin JZ, Rubin LL (2019) Single-cell transcriptomic profiling of the aging mouse brain. *Nat Neurosci* 22:1696–1708.
- Xu L, Ryu J, Nguyen JV, Arena J, Rha E, Vranis P, Hitt D, Marsh-Armstrong N, Koliatsos VE (2015) Evidence for accelerated tauopathy in the retina of transgenic P301S tau mice exposed to repetitive mild traumatic brain injury. *Exp Neurol* 273:168–176.
- Yap JK, Pickard BS, Chan EW, Gan SY (2019) The role of neuronal NLRP1 inflammasome in Alzheimer's disease: bringing neurons into the neuroinflammation game. *Mol Neurobiol* 56:7741–7753.
- Yeates KO (2010) Mild traumatic brain injury and postconcussive symptoms in children and adolescents. *J Int Neuropsychol Soc* 16:953–960.
- Yeates KO, Kaizar E, Rusin J, Bangert B, Dietrich A, Nuss K, Wright M, Taylor HG (2012) Reliable change in postconcussive symptoms and its functional consequences among children with mild traumatic brain injury. *Arch Pediatr Adolesc Med* 166:615–622.
- Yokota T, Mishra M, Akatsu H, Tani Y, Miyauchi T, Yamamoto T, Kosaka K, Nagai Y, Sawada T, Heese K (2006) Brain site-specific gene expression analysis in Alzheimer's disease patients. *Eur J Clin Invest* 36:820–830.
- Zemek R, Barrowman N, Freedman SB, Gravel J, Gagnon I, McGahern C, Aglipay M, Sangha G, Boutis K, Beer D, Craig W, Burns E, Farion KJ, Mikrogianakis A, Barlow K, Dubrovsky AS, Meeuwisse W, Gioia G, Meehan WP, Beauchamp MH, et al. (2016) Clinical risk score for persistent postconcussion symptoms among children with acute concussion in the ED. *JAMA* 315:1014–1025.
- Zhang AL, Sing DC, Rugg CM, Feeley BT, Senter C (2016) The rise of concussions in the adolescent population. *Orthop J Sports Med* 4:2325967116662458.
- Zhong Z, Liang S, Sanchez-Lopez E, He F, Shalpour S, Lin XJ, Wong J, Ding S, Seki E, Schnabl B, Hevener AL, Greenberg HB, Kisseleva T, Karin M (2018) New mitochondrial DNA synthesis enables NLRP3 inflammasome activation. *Nature* 560:198–203.
- Zuckerman SL, Lee YM, Odom MJ, Solomon GS, Forbes JA, Sills AK (2012) Recovery from sports-related concussion: days to return to neurocognitive baseline in adolescents versus young adults. *Surg Neurol Int* 3:130.